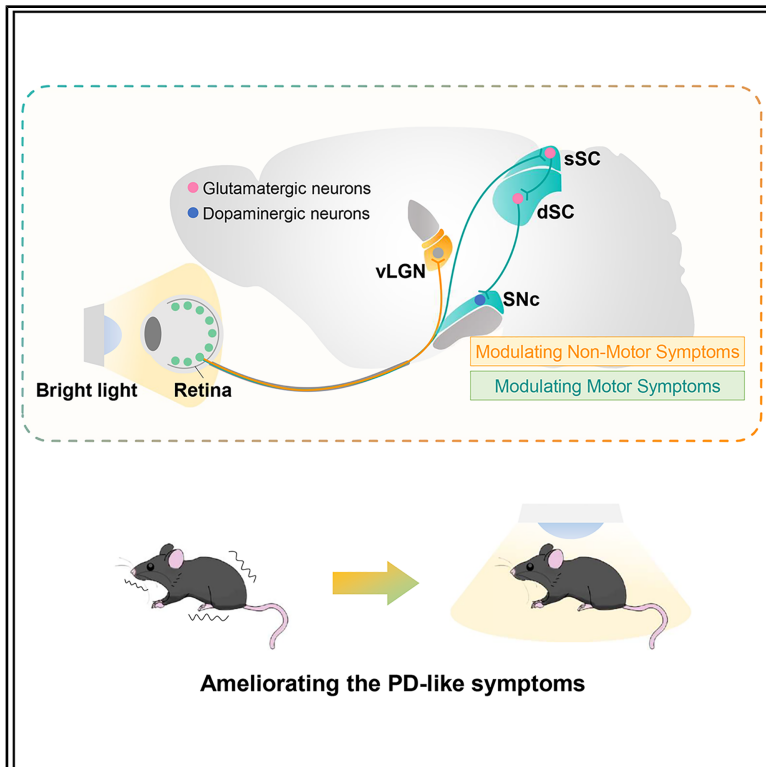


## Bright-light treatment ameliorates motor and non-motor deficits through distinct visual circuits in a mouse model of Parkinson's disease

### Graphical abstract



### Authors

Xiaodan Huang, Shengnan Wang, Zhiqing Chen, ..., Lu Huang, Qian Tao, Chaoran Ren

### Correspondence

huangxd@jnu.edu.cn (X.H.),  
 huanglu@jnu.edu.cn (L.H.),  
 taoqian16@jnu.edu.cn (Q.T.),  
 tchaoran@jnu.edu.cn (C.R.)

### In brief

Huang et al. identified two distinct visual circuits regulating non-motor and motor symptoms of Parkinson's disease. They demonstrated that the vLGN mediates the beneficial effects of bright-light treatment on non-motor symptoms, while the sSC-dSC-SNc pathway alleviates motor symptoms.

### Highlights

- Activation of the vLGN alleviates non-motor symptoms of PD
- Activating SNc-projecting dSC neurons increases SNc dopaminergic neuron-bursting activity
- Glutamatergic sSC neurons directly innervate the dSC-SNc pathway
- Bright-light treatment alleviates PD non-motor and motor symptoms via distinct circuits



## Article

# Bright-light treatment ameliorates motor and non-motor deficits through distinct visual circuits in a mouse model of Parkinson's disease

Xiaodan Huang,<sup>1,10,\*</sup> Shengnan Wang,<sup>1,10</sup> Zhiqing Chen,<sup>1,10</sup> Wenna Qu,<sup>1</sup> Li Song,<sup>2</sup> Zhengfang Hu,<sup>1</sup> Yue Xi,<sup>3</sup> Yan Yang,<sup>1</sup> Weng-Hei Hong,<sup>4</sup> Song Lin,<sup>4</sup> Kwok-Fai So,<sup>1,3,5,6,7</sup> Yulong Li,<sup>8</sup> Lu Huang,<sup>1,\*</sup> Qian Tao,<sup>9,\*</sup> and Chaoran Ren<sup>1,3,5,6,11,\*</sup>

<sup>1</sup>State Key Laboratory of Bioactive Molecules and Druggability Assessment, Guangdong Basic Research Center of Excellence for Natural Bioactive Molecules and Discovery of Innovative Drugs, Department of Neurology and Stroke Center, First Affiliated Hospital of Jinan University, Key Laboratory of CNS Regeneration (Ministry of Education), Guangdong Key Laboratory of Non-human Primate Research, GHM Institute of CNS Regeneration, Jinan University, Guangzhou 510632, China

<sup>2</sup>Experimental Teaching Center of Basic Medicine, School of Basic Medicine and Public Health, Jinan University, Guangzhou 510632, China

<sup>3</sup>Neuroscience and Neurorehabilitation Institute, University of Health and Rehabilitation Sciences, Qingdao, China

<sup>4</sup>Physiology Department, School of Medicine, Jinan University, Guangzhou 510632, China

<sup>5</sup>Co-innovation Center of Neuroregeneration, Nantong University, Nantong 226001, China

<sup>6</sup>Center for Brain Science and Brain-Inspired Intelligence, Guangdong-Hong Kong-Macao Greater Bay Area, Guangzhou 510515, China

<sup>7</sup>Key Laboratory of Brain and Cognitive Science, Li Ka Shing Faculty of Medicine, The University of Hong Kong, Hong Kong SAR, China

<sup>8</sup>State Key Laboratory of Membrane Biology, Peking University School of Life Sciences, Beijing 100871, China

<sup>9</sup>Department of Rehabilitation Medicine, First Affiliated Hospital of Jinan University, Guangzhou, Department of Public Health and Preventive Medicine Psychology, School of Medicine, Jinan University, Guangzhou 510632, China

<sup>10</sup>These authors contributed equally

<sup>11</sup>Lead contact

\*Correspondence: [huangxd@jnu.edu.cn](mailto:huangxd@jnu.edu.cn) (X.H.), [huanglu@jnu.edu.cn](mailto:huanglu@jnu.edu.cn) (L.H.), [taoqian16@jnu.edu.cn](mailto:taoqian16@jnu.edu.cn) (Q.T.), [tchaoran@jnu.edu.cn](mailto:tchaoran@jnu.edu.cn) (C.R.)  
<https://doi.org/10.1016/j.celrep.2025.115865>

## SUMMARY

Light has a profound impact on non-visual functions, and clinical evidence suggests bright-light therapy's effectiveness in alleviating motor and non-motor symptoms of Parkinson's disease (PD). However, the neural mechanisms underlying these effects remain unclear. Here, we demonstrate that bright-light treatment alleviates PD symptoms in mice via distinct visual circuits. Specifically, bright-light signals transmitted by the ventral lateral geniculate nucleus alleviate non-motor symptoms, such as depressive-like behaviors and spatial memory deficits. Conversely, the improvement in motor symptoms with bright-light treatment depends on a separate, disynaptic visual pathway that connects the superficial layers of the superior colliculus to the substantia nigra pars compacta (SNc). Notably, in this pathway, bright-light signals enhance the bursting activity of SNc dopaminergic neurons by upregulating HCN2 expression, a mechanism essential for motor improvements. These findings provide valuable insights into the neural mechanisms by which bright-light therapy benefits PD.

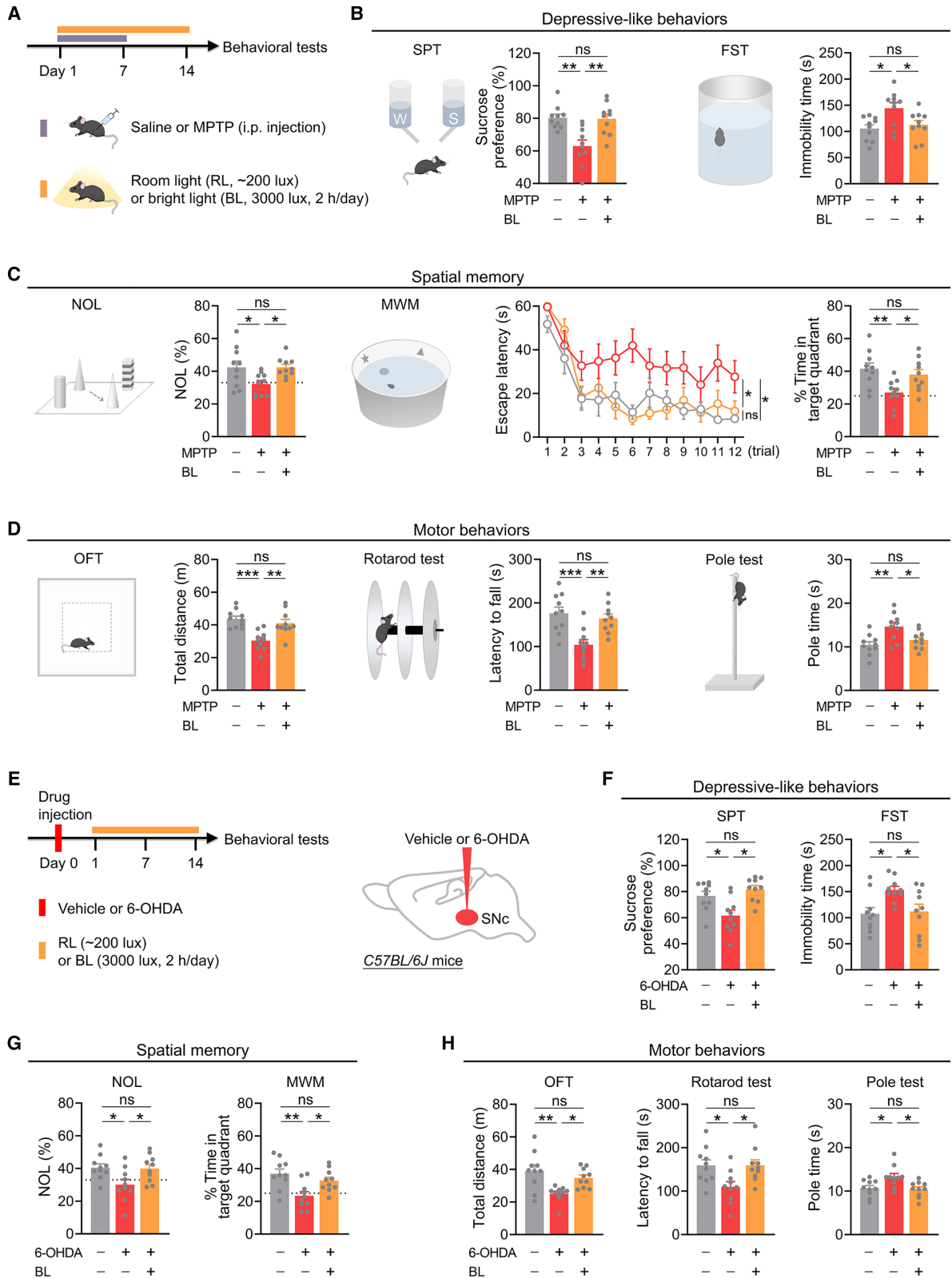
## INTRODUCTION

Light signals in the environment are powerful modulators of physiological and behavioral functions, influencing aspects such as circadian rhythms, mood, cognition, and non-visual sensory perceptions.<sup>1–6</sup> In the clinic, bright-light therapy appears to improve both motor and non-motor symptoms (e.g., depressive symptoms and impairment of cognition) of Parkinson's disease (PD).<sup>7–13</sup> However, the neuronal mechanisms underlying the beneficial effects of bright-light therapy on PD symptoms remain poorly understood.

The regulation of brain functions by light requires the mediation of specific visual-related brain regions. For instance, the suprachiasmatic nucleus (SCN) can mediate the regulatory effects of light on circadian rhythms,<sup>14</sup> while the olivary pretectal nu-

cleus (OPN) is essential for the light-induced pupillary light reflex.<sup>15,16</sup> It is worth noting that recent studies have discovered that the ventral lateral geniculate nucleus (vLGN) in rodents, analogous to the primate pregeniculate nucleus,<sup>17–20</sup> plays a crucial role in mediating the beneficial effects of bright-light treatment on diverse brain functions, including depression relief, memory enhancement, and alleviation of pain and itching behavior.<sup>6,21–25</sup> However, the specific contributions of the vLGN to the modulation of PD symptoms through bright light have yet to be clarified. Furthermore, the potential involvement of other visual-related brain regions in mediating bright light's effects on PD symptoms necessitates comprehensive investigations. In this study, we demonstrate that bright-light treatment ameliorates both motor and non-motor symptoms of PD in mice through distinct visual pathways, elucidating the neural





(legend on next page)

mechanisms underlying the therapeutic effects of bright-light treatment in PD.

## RESULTS

### Bright-light treatment alleviates depressive-like behaviors, enhances spatial memory, and improves motor deficits in PD mouse models

Motor and non-motor deficits are prevalent in PD.<sup>26</sup> To assess the potential modulatory effects of bright-light treatment on these symptoms, we initially established a mouse model of PD by daily intraperitoneal (i.p.) injection of 1-methyl-4-phenyl-1,2,3,6-tetrahydropyridine (MPTP) (30 mg/kg) for 7 consecutive days (Figure 1A). We examined PD-like non-motor symptoms, with a particular focus on depressive-like behaviors and spatial memory deficits at 1 week after MPTP administration (Figure 1A). MPTP-treated mice exhibited increased depressive-like behaviors, as evidenced by decreased preference in the sucrose preference test (SPT) and increased immobility in the forced swimming test (FST) (Figure 1B). In memory assessments, the novel location recognition test (NOL) revealed that mice receiving MPTP treatment explored the novel location by chance, indicating the impairment of spatial memory (Figures 1C and S1A). This deficit was further supported by their performance in the Morris water maze (MWM), where they displayed prolonged escape latency and reduced engagement with the target quadrant (Figures 1C and S1A). Additionally, significant motor deficits were observed in these mice, including decreased locomotion in the open-field test (OFT), reduced latency to fall in the rotarod test, and increased time on the pole test (Figure 1D). These results suggest that MPTP treatment could cause mice to exhibit both motor and non-motor symptoms of PD.

To evaluate the effects of bright-light treatment on these PD symptoms, experimental mice received daily bright-light treatment (3,000 lux) from zeitgeber time 1 (ZT1) to ZT3 for 2 weeks. Concurrently, they received daily i.p. injection of MPTP during the first week (Figure 1A). After 2 weeks of bright-light treatment, we found that bright-light treatment alleviated depressive-like behaviors, enhanced spatial memory, and improved motor deficits in MPTP-treated mice (Figures 1B–1D and S1A). These beneficial effects were further confirmed in an additional mouse model of PD induced by acute bilateral injections of 6-hydroxydopamine (6-OHDA) into the SNc<sup>27,28</sup> (Figures 1E–1H, S1B, and S1C).

Next, we probed the dosage effects of bright-light treatment on PD symptoms. We compared the effects of 1 week, 2 weeks, and 3 weeks of bright-light treatment (3,000 lux, 2 h/day) on both

the non-motor and motor symptoms of MPTP-treated mice (Figure S1D). The beneficial effects of bright-light treatment appear to be dose dependent, and at least 2 weeks of bright-light treatment was needed to significantly ameliorate both the non-motor and motor symptoms of MPTP-treated mice (Figures S1E–S1G). Finally, we tested whether bright-light treatment could reverse PD symptoms induced by MPTP. We used a 21-day protocol in which 2 weeks of bright-light treatment (3,000 lux, 2 h/day) were conducted following 7 days of i.p. injection of MPTP (Figure S1H). We found that bright-light treatment reversed both the non-motor and motor symptoms induced by MPTP (Figures S1I–S1K).

### Activation of the vLGN is required for the beneficial effects of bright-light treatment on non-motor symptoms in a PD mouse model

The vLGN has been demonstrated to play a crucial role in mediating the beneficial effects of bright-light treatment on various brain functions, including alleviating depressive symptoms and enhancing memory.<sup>6,21,22,24</sup> To explore whether the vLGN contributes to the beneficial effects of bright-light treatment on PD symptoms, we firstly assessed how bright light influences neuronal activity in the vLGN. We injected adeno-associated virus (AAV) encoding calmodulin-based genetically encoded green fluorescent protein calcium indicators (GCaMP7s) into the vLGN of C57BL/6J mice and implanted an optical fiber above the injection site (Figure 2A). Using fiber photometry, we quantitatively measured the changes in Ca<sup>2+</sup> signals induced by bright-light stimulation (3,000 lux, 2 s/trial) in vLGN neurons (Figure 2A). Bright light consistently provoked a robust increase in Ca<sup>2+</sup> signals in these neurons (Figure 2B), confirming that bright light activates the vLGN. Subsequently, we investigated whether activating the vLGN is essential for the beneficial effects of bright-light treatment on both non-motor and motor symptoms in the MPTP-induced PD mouse model. To selectively inhibit neuronal activity in the vLGN during bright-light treatment, we employed chemogenetic approaches utilizing designer receptors exclusively activated by designer drugs (DREADDs). AAV vectors carrying neuron-specific inhibitory DREADDs fused with mCherry (AAV2/9-human synapsin [hSyn]-hM4Di-mCherry) were injected bilaterally into the vLGN (Figures 2C and 2D). Two weeks later, we chemogenetically inhibited the vLGN neurons daily by i.p. injection of clozapine *N*-oxide (CNO, 1 mg/kg) 30 min before bright-light treatment (3,000 lux, 2 h/day for 2 weeks) (Figure 2C). The inhibition of vLGN neurons significantly impaired the beneficial effects of bright-light treatment on depressive-like symptoms and spatial memory (Figures 2E, 2F, and S2A). However, this inhibition did not significantly affect

### Figure 1. Bright-light treatment alleviates depressive-like behaviors, enhances spatial memory, and improves motor deficits in PD mouse models

(A) Experimental design.

(B–D) Depressive-like behaviors tested in the SPT and FST (B), spatial memory tested in the NOL and MWM (C), and motor behaviors tested in the OFT, rotarod test, and pole test (D) (*n* = 10 mice/group).

(E) Experimental design.

(F–H) Depressive-like behaviors tested in the SPT and FST (F), spatial memory tested in the NOL and MWM (G), and motor behaviors tested in the OFT, rotarod test, and pole test (H) (*n* = 10 mice/group).

Error bars indicate SEM. One-way ANOVA with Sidak's multiple comparisons test: \**p* < 0.05, \*\**p* < 0.01, \*\*\**p* < 0.001; ns, not significant. See also Figure S1.

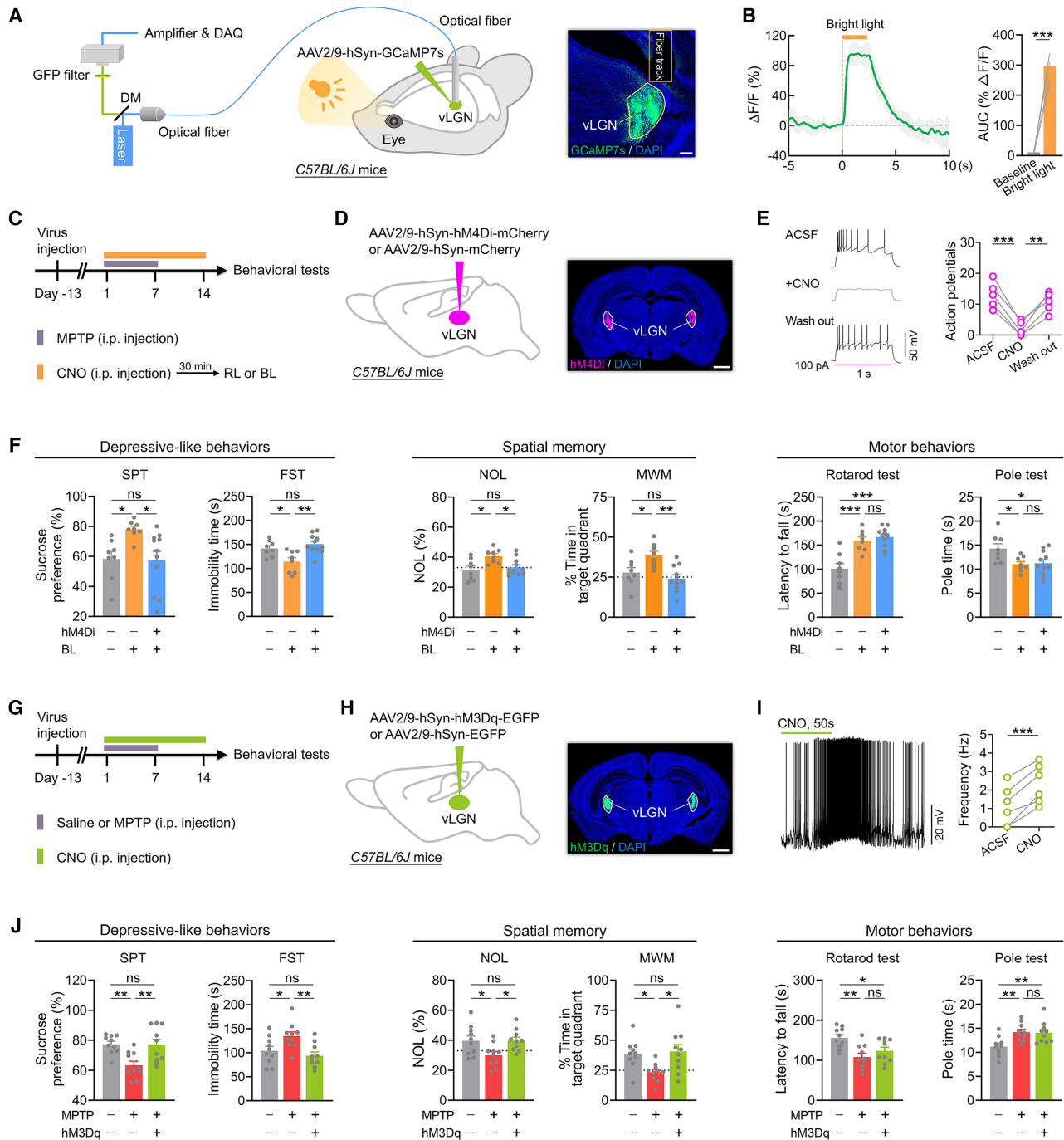


**Figure 2. Activation of the vLGN is required for the beneficial effects of bright-light treatment on non-motor symptoms in PD mouse model**

(A) Schematic diagram (left) and representative image (right) illustrate the expression of GCaMP7s and the placement of optical fiber in the vLGN.

(B) Average responses and area under the curve (AUC) of  $Ca^{2+}$  signals in vLGN neurons in response to bright-light stimulation.

(C) Experimental design.

(D) Specific labeling of vLGN neurons with hM4Di-mCherry or mCherry in *C57BL/6J* mice.

(E) Functional validation of chemogenetic inhibition in hM4Di-expressing vLGN neurons. ACSF, artificial cerebrospinal fluid.

(F) Depressive-like behaviors tested in the SPT and FST, spatial memory tested in the NOL and MWM, and motor behaviors tested in the rotarod test and pole test ( $n = 8-10$  mice/group). All mice received daily intraperitoneal (i.p.) injection of MPTP (30 mg/kg) for 7 consecutive days and daily i.p. injection of CNO (1 mg/kg) for 2 weeks.

(G) Experimental design.

(H) Specific labeling of vLGN neurons with hM3Dq-EGFP or EGFP in *C57BL/6J* mice.

(legend continued on next page)

the beneficial effects of bright-light treatment on motor symptoms (Figures 2F and S2B). These results suggest that while the transmission of bright-light signals by the vLGN is essential for improving non-motor symptoms in MPTP-treated mice, it does not impact motor symptoms.

To further verify the vLGN's role in the regulation of PD symptoms, we evaluated the effects of activating vLGN neurons on both non-motor and motor symptoms in MPTP-treated mice. Neuronal activator DREADD hM3Dq and enhanced green fluorescent protein (EGFP) were expressed in vLGN neurons (Figures 2G and 2H). We then activated the infected neurons daily with an i.p. injection of CNO (1 mg/kg) for 14 days (Figures 2G and 2I). Activating vLGN neurons significantly reduced depressive-like behaviors and enhanced spatial memory in MPTP-treated mice (Figures 2J and S2C) yet had no significant impact on motor symptoms (Figures 2J and S2D). Together, these findings confirm that activation of the vLGN is crucial for the antidepressant and spatial-memory-promoting effects of bright-light treatment in MPTP-treated mice, but not for improving motor deficits. This suggests that other visual-related brain regions may mediate the beneficial effects of bright-light treatment on motor symptoms.

### Enhanced bursting activity of surviving SNc dopaminergic neurons is required for the beneficial effects of bright-light treatment on motor symptoms of PD

Given the well-established correlation between the progressive dysfunction and death of dopaminergic neurons in the SNc and deficits in motor functions in PD,<sup>29,30</sup> we investigated whether bright-light treatment could mitigate the motor symptoms in PD mice by influencing the morphological and/or physiological characteristics of SNc dopaminergic neurons. Initially, we assessed how bright light affects the neuronal activity of these neurons. We injected Cre-dependent AAVs encoding GCaMP7s into the SNc of *DAT-Cre* mice (Figure 3A). Fiber photometry recordings demonstrated a consistent increase in Ca<sup>2+</sup> signals in SNc dopaminergic neurons at the onset of the bright-light stimulation (Figure 3A), suggesting that bright light activates SNc dopaminergic neurons. Subsequently, we examined whether bright-light treatment influences the MPTP-induced loss of SNc dopaminergic neurons. After 2 weeks of bright-light treatment, we found no significant changes in the decreased number of tyrosine-hydroxylase-positive (TH<sup>+</sup>) neurons in the SNc (Figure 3B) and reduction of SNc-to-DS (dorsal striatum) projections (Figure 3C). These results suggest that bright-light treatment does not significantly ameliorate the morphological abnormalities in SNc dopaminergic neurons caused by MPTP treatment.

To determine how bright-light treatment influences physiological functions of surviving SNc dopaminergic neurons following MPTP administration, we expressed enhanced yellow fluores-

cent protein (eYFP) in SNc dopaminergic neurons of *DAT-Cre* mice. Whole-cell patch-clamp recordings were subsequently performed on eYFP-labeled neurons within the SNc to characterize their action potential firing patterns. Consistent with previous findings,<sup>31</sup> SNc dopaminergic neurons exhibited intrinsic activity patterns that included silent, tonic, and burst firing (Figure 3D). We observed a significant reduction in burst-firing neurons, from 28.2% in wild-type controls to just 2.8% in MPTP-treated mice (Figure 3D). However, 2 weeks of bright-light treatment significantly restored the percentage of burst-firing neurons (Figure 3D), indicating that long-term exposure to bright light enhances burst firing in SNc dopaminergic neurons.

Since burst firing is strongly associated with dopamine release<sup>32</sup> and considering that SNc dopaminergic neurons are critical for motor regulation via their dopamine release in the DS,<sup>33</sup> we further investigated how bright-light treatment influences dopamine release in the DS following MPTP treatment. To monitor dopamine release, we expressed genetically encoded GPCR-activation-based dopamine sensor (GRAB-DA sensor)<sup>34</sup> that reports dopamine dynamics in the DS (Figure 3E). MPTP treatment significantly reduced dopamine release during treadmill running, which was restored by bright-light treatment (Figure 3E). These findings suggest that bright-light treatment enhances the physiological function of SNc dopaminergic neurons.

Given the established role of the postsynaptic *N*-methyl-D-aspartate receptors (NMDARs), low-voltage-sensitive T-type calcium channels (T-VSCCs), and the hyperpolarization-activated cyclic nucleotide-gated (HCN) channels in regulating neuronal bursting activity,<sup>35</sup> we explored whether any of these proteins are essential for the effects of bright-light treatment on bursting activity in SNc dopaminergic neurons. To this end, we expressed eYFP in SNc dopaminergic neurons of *DAT-Cre* mice and applied specific antagonists to SNc brain slices from these MPTP-treated *DAT-Cre* mice that had undergone 2 weeks of bright-light treatment: the NMDAR antagonist 2-amino-5-phosphonovaleric acid (AP5, 100  $\mu$ M), the T-VSCC blocker mibefradil (10  $\mu$ M), and the HCN channel antagonist ZD7288 (50  $\mu$ M). ZD7288 significantly reduced bursting activity in SNc dopaminergic neurons (Figure 3F), while AP5 had a moderate but smaller impact compared to ZD7288 (Figure 3F). Conversely, mibefradil did not notably alter bursting activity (Figure 3F). Additionally, we observed a 68.3%  $\pm$  18.9% reduction in the levels of HCN2 protein—a subunit of the HCN family—in SNc brain tissues from the MPTP-treated group compared to wild-type controls (Figure 3G). Moreover, this reduction was partially reversed in MPTP-treated mice that received bright-light treatment (Figure 3G). These results suggest that bright-light treatment could enhance the bursting activity in SNc dopaminergic neurons by upregulating HCN2 expression.

To further assess the role of enhanced bursting activity in SNc dopaminergic neurons in mediating the beneficial effects of bright-light treatment on PD symptoms, we first examined

(I) Functional validation of chemogenetic activation in hM3Dq-expressing vLGN neurons.

(J) Depressive-like behaviors tested in the SPT and FST, spatial memory tested in the NOL and MWM, and motor behaviors tested in the rotarod test and pole test ( $n = 10$  mice/group). All mice received daily i.p. injection of CNO (1 mg/kg) for 2 weeks and exposure to room light (RL, 200 lux) during the daytime.

Scale bars, 200  $\mu$ m (A) and 1 mm (D and H). Error bars indicate SEM. One-way ANOVA with Sidak's multiple comparisons test: \* $p < 0.05$ , \*\* $p < 0.01$ , \*\*\* $p < 0.001$ ; ns, not significant. See also Figure S2.

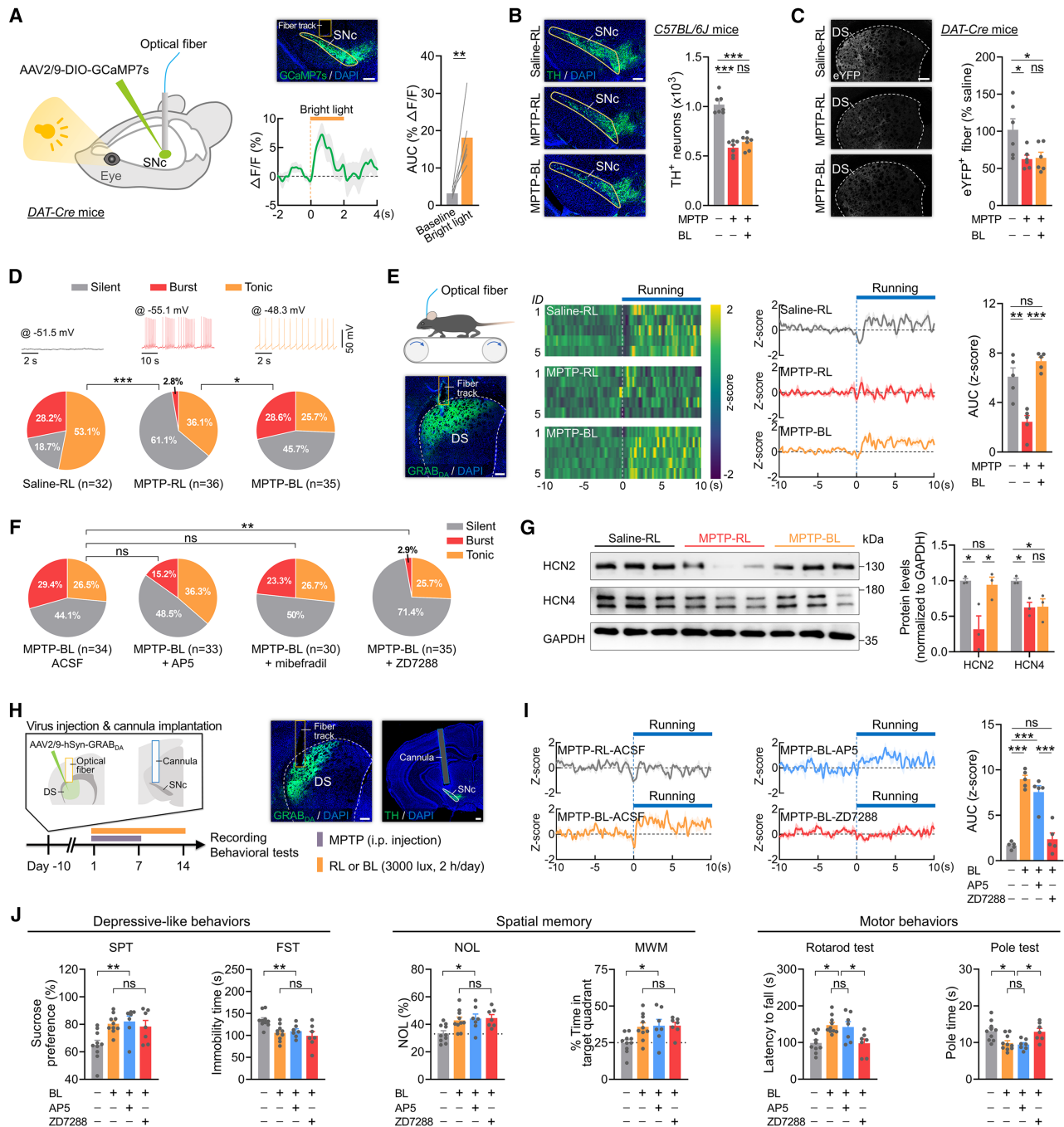


**Figure 3. Enhanced bursting activity of surviving SNc dopaminergic neurons is required for the beneficial effects of bright-light treatment on motor symptoms of PD**

(A) Left: specific labeling of SNc dopaminergic neurons with GCaMP7s in *DAT-Cre* mice. Right: average responses and AUC of  $Ca^{2+}$  signals in SNc dopaminergic neurons in response to bright-light stimulation ( $n = 6$  mice).

(B) Representative images and the number of SNc TH<sup>+</sup> neurons in different experimental groups ( $n = 7$  mice/group).

(C) Representative images of axonal terminals of SNc dopaminergic neurons in the DS of *DAT-Cre* mice, and the average projection density in different experimental groups ( $n = 6$  mice/group).

(D) Top: representative traces showing spontaneous activity of silent, tonic-firing, and burst-firing SNc dopaminergic neurons. Bottom: pie charts indicating percentage of the three types of SNc dopaminergic neurons in different experimental groups ( $n = 32$ – $36$  cells/group).

(E) Left: representative image showing the optical-fiber track positioned above the DS neurons expressing GRAB<sub>DA</sub> sensor. Right: heatmaps, average traces, and AUC of dopamine dynamics in the DS during treadmill running in different experimental groups ( $n = 5$  mice/group).

(legend continued on next page)

whether inhibiting bursting activity in SNc neurons could impact dopamine release in the DS of MPTP-treated mice that received bright-light treatment (Figure 3H). Thirty minutes after infusing either AP5 (1  $\mu$ g, 150 nL/site)<sup>36</sup> or ZD7288 (0.1  $\mu$ g, 150 nL/site)<sup>37</sup> into the SNc, we found that ZD7288 infusion significantly impaired the effects of bright-light treatment on dopamine release during treadmill running, while AP5 had minimal impact (Figure 3I). Next, we tested the contribution of NMDAR and HCN channels in the SNc to the beneficial effects of bright-light treatment on MPTP-induced PD symptoms. We infused AP5 or ZD7288 bilaterally into the SNc of MPTP-treated mice following bright-light treatment (Figures 3H and S3A). AP5 infusion did not significantly alter the beneficial effects of bright-light treatment on either motor or non-motor symptoms induced by MPTP (Figures 3J, S3B, and S3C). However, while ZD7288 infusion in the SNc did not significantly affect the improvement in non-motor symptoms (Figures 3J and S3B), it abolished the beneficial effects of bright-light treatment on motor symptoms (Figures 3J and S3C). These findings indicate that enhanced bursting activity in SNc dopaminergic neurons, facilitated by increased HCN2 expression, plays a crucial role in alleviating motor symptoms through bright-light treatment.

#### Activation of SNc-projecting dSC neurons is required for the beneficial effects of bright-light treatment on motor symptoms in a PD mouse model

To identify potential brain regions that might relay light signals to SNc dopaminergic neurons, we conducted a retrograde trans-monosynaptic tracing experiment by injecting Cre-dependent helper viruses expressing the rabies glycoprotein and histone-tagged mCherry (Helper-mCherry) into the SNc of *DAT-Cre* mice. After 3 weeks, EnvA-pseudotyped rabies virus (RV)- $\Delta$ G-EGFP was injected into the same site (Figures 4A and 4B). The presence of these helper viruses facilitates monosynaptic retrograde RV spread.<sup>38</sup> EGFP-labeled neurons were examined in several visual-related brain regions, including the SCN, vLGN, and superior colliculus (SC) (Figure 4C). We found that only neurons in deep layers of the SC (dSC) showed synaptic convergence onto SNc dopaminergic neurons (Figure 4C). Additionally, fiber photometry recordings revealed that SNc-projecting dSC neurons could be activated by bright-light stimulation (Figure 4D) and that chemogenetic inhibition of dSC neurons significantly impaired the excitatory effects of bright light on SNc dopaminergic neurons (Figure S4A). These findings suggest that bright-light treatment could regulate neuronal activity of SNc dopaminergic neurons by activating the dSC.

To investigate whether SNc-projecting dSC neurons contribute to the beneficial effects of bright-light treatment on

PD symptoms, we assessed depressive-like behaviors, spatial memory, and motor behaviors in MPTP-treated mice after chemogenetic inhibition of these neurons during bright-light treatment (Figure 4E). We delivered the monosynaptic retrograde transport virus rAAV2/2-Retro-Cre along with AAV2/9-DIO-eYFP into the SNc of *DAT-Cre* mice to infect SNc-projecting dSC neurons with AAV2/9-DIO-hm4Di-mCherry and label SNc dopaminergic neurons with eYFP (Figure 4F). While chemogenetic inhibition of SNc-projecting dSC neurons did not significantly impact bright-light treatment's beneficial effects on depressive-like behaviors and spatial memory (Figures 4H and S4B), it significantly impaired the effects on motor symptoms and bursting activity in SNc dopaminergic neurons in MPTP-treated mice (Figures 4H, 4I, and S4C). Furthermore, Selective inhibition of SNc-projecting dSC neurons in wild-type control animals did not significantly alter motor performance in the OFT, rotarod test, or pole test (Figures S4D and S4E), suggesting that the effect of inhibiting dSC neurons on bright-light treatment's efficacy in improving motor symptoms is not due to changes in the dSC's own regulatory role on motor functions. Together, these results indicate that activation of SNc-projecting dSC neurons is essential for the improvement of motor symptoms through bright-light treatment.

#### dSC neurons activate SNc dopaminergic neurons through direct projections

To determine how the dSC regulates neuronal activity in SNc dopaminergic neurons, we injected AAV2/9-DIO-eYFP into the SNc of *DAT-Cre* mice and delivered AAVs encoding channelrhodopsin-2 and mCherry (AAV2/9-hSyn-ChR2-mCherry) into the dSC (Figure 5A). We then performed whole-cell recordings from eYFP-labeled neurons in the SNc (Figure 5B). Optogenetically activating the ChR2-expressing dSC-to-SNc projections evoked exclusively excitatory postsynaptic currents (EPSCs) in 52.8% of recorded neurons but both EPSCs and inhibitory postsynaptic currents (IPSCs) in 1.9% of recorded neurons (Figure 5C). The EPSCs could be blocked by tetrodotoxin (TTX) and restored by potassium channel blocker 4-aminopyridine (4-AP) (Figure 5D). Furthermore, EPSCs could be blocked by application of 6-cyano-7-nitroquinoxaline-2,3-dione (CNQX), a selective AMPA/kainate receptor antagonist (Figure 5E). These results demonstrate that dSC neurons form monosynaptic glutamatergic synapses with SNc dopaminergic neurons. To further confirm whether SNc dopaminergic neurons receive direct inputs from the dSC, we delivered the monosynaptic anterograde transport virus AAV2/1-Cre<sup>39</sup> into the dSC of *C57BL/6J* mice and infected SNc postsynaptic neurons with AAV2/9-DIO-eYFP (Figures S5D and S5E). eYFP-labeled neurons were mainly

(F) Pie charts indicating percentage of the three types of SNc dopaminergic neurons in different experimental groups ( $n = 30$ –35 cells/group).

(G) Representative bands and quantitative data showing HCN2 and HCN4 protein expression in different experimental groups ( $n = 3$  mice/group).

(H) Left: experimental design. Right: representative images showing virus expression within the DS and cannula implantation in the SNc of *C57BL/6J* mice.

(I) Average traces and the AUC of dopamine dynamics during treadmill running in different experimental groups ( $n = 5$  mice/group). All mice received daily i.p. injection of MPTP (30 mg/kg) for 7 consecutive days and received an infusion of drug into the SNc 30 min prior to recording and behavioral tests.

(J) Depressive-like behaviors tested in the SPT and FST, spatial memory tested in the NOL and MWM, and motor behaviors tested in the rotarod test and pole test ( $n = 7$ –10 mice/group).

Scale bars, 100  $\mu$ m (A [middle] and B [left]) and 200  $\mu$ m (C [left], E [left], and H). Error bars indicate SEM. One-way ANOVA with Sidak's multiple comparisons test (A–C, E, G, I, and J) and chi-squared test (D and F): \* $p < 0.05$ , \*\* $p < 0.01$ , \*\*\* $p < 0.001$ ; ns, not significant. See also Figure S3.

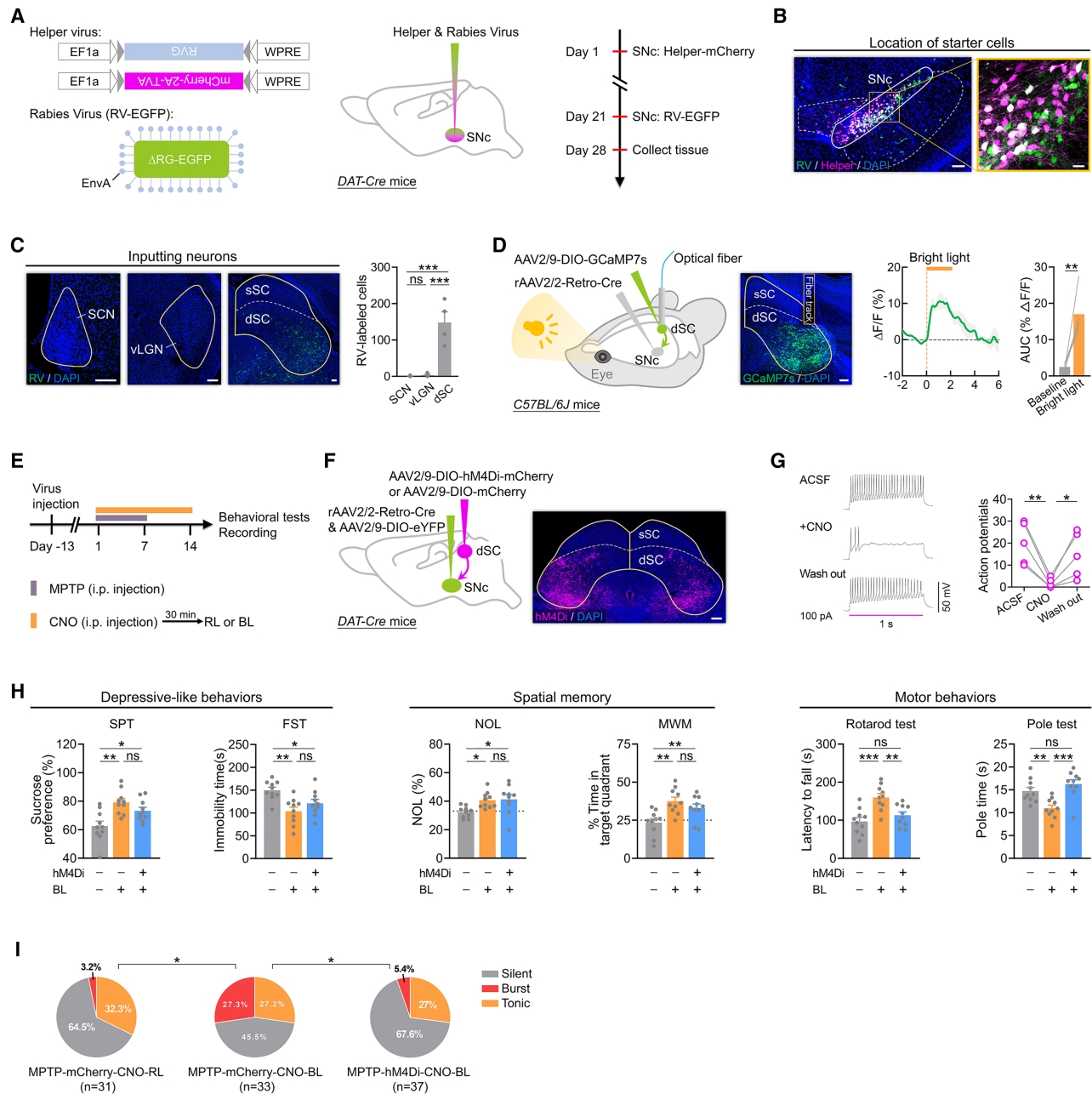


**Figure 4. Activation of SNc-projecting dSC neurons is required for the beneficial effects of bright-light treatment on motor symptoms in PD mouse model**

(A) Experimental design of virus tracing in *DAT-Cre* mice.  
 (B) Injection site of the SNc illustrating the location of starter cells (white).  
 (C) RV-EGFP-labeled neurons in the SCN, vLGN, and SC.  
 (D) Left: specific labeling of SNc-projecting dSC with GCaMP7s. Right: average responses and AUC of  $Ca^{2+}$  signals in response to bright-light stimulation ( $n = 5$  mice).  
 (E) Experimental design.  
 (F) Specific labeling of SNc-projecting dSC neurons with hM4Di-mCherry or mCherry, and SNc dopaminergic neurons with eYFP in *DAT-Cre* mice.  
 (G) Functional validation of chemogenetic inhibition in SNc-projecting dSC neurons expressing hM4Di.  
 (H) Depressive-like behaviors tested in the SPT and FST, spatial memory tested in the NOL and MWM, and motor behaviors tested in the rotarod test and pole test ( $n = 10$  mice/group). All mice received daily i.p. injection of MPTP (30 mg/kg) for 7 consecutive days and daily i.p. injection of CNO (1 mg/kg) for 2 weeks.  
 (I) Pie charts indicating percentage of the three types of SNc dopaminergic neurons in different experimental groups ( $n = 31-37$  cells/group).  
 Scale bars, 25  $\mu$ m (B [right]), 100  $\mu$ m (B [left] and C), and 200  $\mu$ m (D and F). Error bars indicate SEM. One-way ANOVA with Sidak's multiple comparisons test (C, D, G, and H) and chi-squared test (I): \* $p < 0.05$ , \*\* $p < 0.01$ , \*\*\* $p < 0.001$ ; ns, not significant. See also Figure S4.

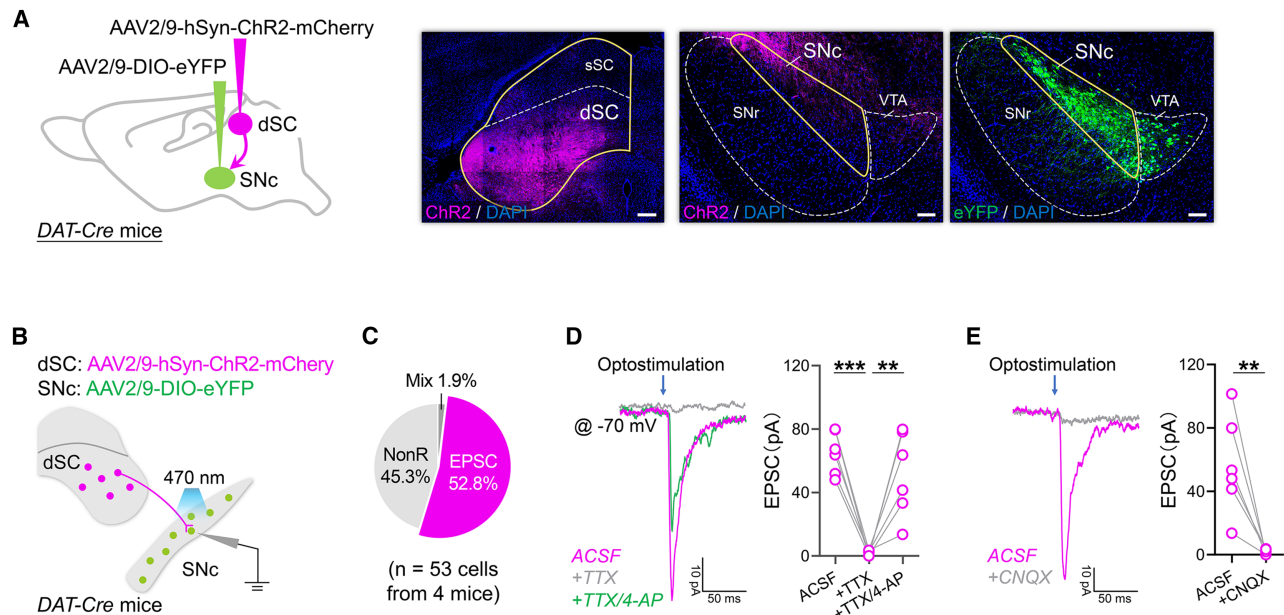


**Figure 5. dSC neurons activate the SNc through direct projections**

(A) Specific labeling of dSC neurons with Chr2-mCherry and SNc dopaminergic neurons with eYFP in *DAT-Cre* mice. (B) Scheme for recording the optogenetically evoked postsynaptic currents in eYFP-expressing SNc neurons. (C) Pie chart indicating whether the absolute amplitude was greater for evoked EPSCs, IPSCs and EPSCs (Mix), or no response (NonR). (D and E) Optogenetically evoked postsynaptic currents recorded from eYFP-expressing SNc neurons. Scale bars, 100  $\mu$ m (A [middle and right]) and 200  $\mu$ m (A [left]). Error bars indicate SEM. One-way ANOVA with Sidak's multiple comparisons test: \*\* $p < 0.01$ , \*\*\* $p < 0.001$ . See also Figure S5.

located in the lateral part of the SNc (Figure S5D), in which approximately 96.7% of these neurons were immunopositive for TH (Figure S5F). The above results indicate that a subset of dSC glutamatergic neurons activate SNc dopaminergic neurons through direct projections.

### Activation of the dSC-SNc pathway ameliorates motor deficits in a PD mouse model

To explore whether long-term activation of the dSC-SNc pathway could mitigate motor symptoms in MPTP-treated mice, we initially selectively expressed hM3Dq on SNc-projecting dSC neurons and labeled SNc dopaminergic neurons with mCherry (Figures 6A and 6B). SNc-projecting dSC neurons were then activated daily through i.p. injection of CNO (1 mg/kg) for 2 weeks (Figures 6A and 6C). Long-term activation of SNc-projecting dSC neurons significantly improved motor symptoms in MPTP-treated mice, accompanied by enhanced bursting activity in SNc dopaminergic neurons (Figures 6D and 6E).

To further determine the contribution of the dSC-SNc pathway in bright-light treatment's effects on motor symptoms, we injected AAV2/1-Flippase (Flpo) into the bilateral dSC and targeted postsynaptic SNc dopaminergic neurons with AAV2/9-fDIO-hM3Dq-EGFP<sup>40</sup> in *DAT-Cre* mice (Figure 6F). Long-term activation of SNc dopaminergic neurons that received direct dSC inputs also significantly improved motor symptoms, accompanied by enhanced bursting activity in these neurons (Figures 6G–6I). Together, long-term activation of the dSC-SNc pathway is sufficient to ameliorate motor symptoms induced by MPTP.

### Activation of dSC-projecting sSC neurons is required for the beneficial effects of bright-light treatment on motor deficits in a PD mouse model

To identify potential brain regions that might relay bright-light signals to the dSC-SNc pathway, we infected dSC neurons with AAVs expressing the rabies glycoprotein and histone-tagged EGFP (Helper-EGFP). EnvA-pseudotyped RV- $\Delta$ G-DsRed<sup>41,42</sup> was then injected into the SNc to infect Helper<sup>+</sup> SNc-projecting dSC neurons via their presynaptic terminals (Figures 7A–7C). DsRed-labeled neurons were examined in the retina, SCN, vLGN, and SC. We found that only neurons in the superficial layers of the SC (sSC) were labeled with RV-DsRed (Figure 7D), and approximately 93.5% of these neurons were immunopositive for glutamate (Figure S6A). Additionally, fiber photometry recordings revealed that dSC-projecting sSC neurons could be activated by bright-light stimulation (Figure 7E), and chemogenetic inhibition of sSC neurons significantly impaired the excitatory effects of bright-light stimulation on SNc-projecting dSC neurons (Figures 7F and S6B). These findings suggest that bright-light treatment could regulate neuronal activity in the dSC-SNc pathway through activating the sSC.

To investigate whether dSC-projecting sSC neurons contribute to the beneficial effects of bright-light treatment on motor symptoms, we assessed motor behaviors in MPTP-treated mice after chemogenetic inhibition of these neurons during bright-light treatment (Figure 7G). We delivered rAAV2/2-Retro-Cre into the bilateral dSC and infected dSC-projecting sSC neurons with AAV2/9-DIO-hM4Di-mCherry (Figure 7G).

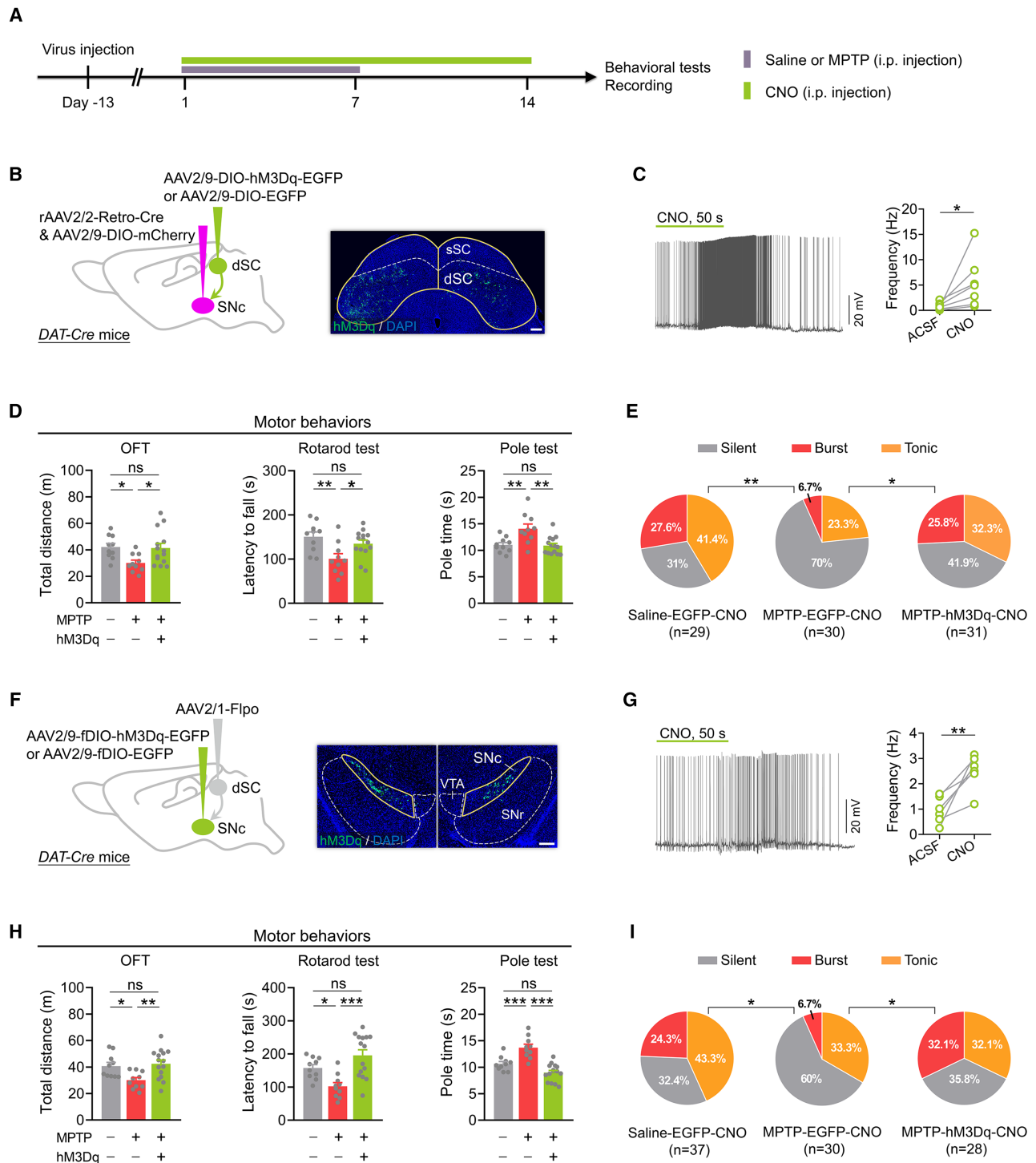


**Figure 6. Activation of the dSC-SNc pathway ameliorates motor deficits in PD mouse model**

(A) Experimental design.

(B) Specific labeling of SNc-projecting dSC neurons with hM3Dq-EGFP or EGFP, and SNc dopaminergic neurons with mCherry in *DAT-Cre* mice.

(C) Functional validation of chemogenetic activation in SNc-projecting dSC neurons expressing hM3Dq.

(D) Motor behaviors tested in the OFT, rotarod test, and pole test ( $n = 10-14$  mice/group). All mice received daily i.p. injection of CNO (1 mg/kg) for 2 weeks.

(E) Pie charts indicating percentage of the three types of SNc dopaminergic neurons in different experimental groups ( $n = 29-31$  cells/group).

(F) Specific labeling of SNc dopaminergic neurons receiving direct dSC inputs with hM3Dq-EGFP or EGFP in *DAT-Cre* mice.

(G) Functional validation of chemogenetic activation in hM3Dq-expressing SNc dopaminergic neurons receiving direct dSC inputs.

(legend continued on next page)

Inhibition of dSC-projecting sSC neurons significantly impaired the beneficial effects of bright-light treatment on motor symptoms (Figures 7H and S6C).

When we tested the effects of long-term activation of dSC-projecting sSC neurons on motor symptoms in MPTP-treated mice, we found that 2 weeks of chemogenetic activation of dSC-projecting sSC neurons significantly improved the motor deficits of MPTP-treated mice in the OFT, rotarod test, and pole test (Figures 7I, 7J, and S6D). These results indicate that long-term activation of dSC-projecting sSC neurons improve the motor symptoms of the PD mouse model.

## DISCUSSION

Bright-light treatment has demonstrated beneficial effects on various brain functions, including mood, cognition, sensory perceptions, and sleep.<sup>21–23,25,43</sup> Clinical evidence supports the efficacy of bright-light therapy in alleviating both non-motor and motor symptoms of PD,<sup>7–13</sup> yet the neuronal mechanisms underlying these effects are not well understood. In this study, we elucidate the role of the vLGN in mediating the beneficial effects of bright-light treatment on mood- and memory-related non-motor deficits in a PD mouse model. Moreover, we provide direct evidence that bright-light treatment can improve motor deficits of PD through a disynaptic visual pathway linking the sSC and the SNc.

The vLGN has been currently identified as a key contributor to the beneficial effects of bright-light treatment on diverse brain functions.<sup>21–23,25</sup> Given that bright-light treatment improves mood disturbances, cognitive impairments, and motor deficits in both patients with PD<sup>7–13</sup> and PD animal models (Figures 1 and S1), we postulate that the vLGN may also play a pivotal role in mediating the beneficial effects of bright-light treatment on PD symptoms. Supporting this hypothesis, we demonstrate that inhibition of the vLGN during bright-light treatment significantly diminishes its positive impact on non-motor symptoms, such as increased depressive-like behaviors and impaired spatial memory (Figures 2F and S2A). Conversely, prolonged activation of vLGN neurons enhances the improvement of non-motor symptoms in our PD mouse model (Figures 2J and S2B). These findings strongly suggest that bright-light signals may be conveyed through pathways related to the vLGN to mitigate non-motor symptoms in the PD mouse model and implies that other visual-related brain regions are involved in mediating the effects of bright-light treatment on motor symptoms. Consistently, we have shown that a disynaptic pathway connecting the sSC and the SNc contributes to the beneficial effects of bright-light treatment on motor symptoms in the PD mouse model.

Bright light can activate SNc dopaminergic neurons (Figure 3A).<sup>44,45</sup> Considering that SNc dopaminergic neurons project to the DS, crucial for motor function via dopamine release,<sup>33,46,47</sup> and their impairment is linked to PD motor symp-

oms,<sup>29,30</sup> we hypothesize that bright-light treatment may alleviate motor symptoms in a PD mouse model by influencing the morphological and/or physiological properties of SNc dopaminergic neurons. Supporting this hypothesis, while bright-light treatment did not significantly correct the morphological abnormalities, it enhanced bursting activity in these neurons (Figures 3B–3D) and increased dopamine release in the DS of MPTP-treated mice (Figure 3E).

Dysfunction of HCN channels in SNc dopaminergic neurons has been reported across various PD mouse models.<sup>48–50</sup> In this study, we also observed a reduction in bursting activity of SNc dopaminergic neurons accompanied by decreased HCN2 expression (Figures 3D and 3G). Notably, we demonstrated that bright-light treatment enhances burst firing in SNc dopaminergic neurons by upregulating HCN2 expression in the SNc (Figures 3H–3J). Moreover, our findings indicate that increased bursting activity in SNc dopaminergic neurons is crucial for the beneficial effects of bright-light treatment on motor symptoms (Figures 3H–3J). Collectively, these results strongly suggest that bright-light treatment may alleviate PD motor symptoms by enhancing the bursting activity of surviving SNc dopaminergic neurons.

Previous research suggests that SNc dopaminergic neurons are implicated in regulating depressive-like behaviors.<sup>51,52</sup> Intriguingly, we found that reducing bursting activity in SNc neurons impaired only the beneficial effects of bright-light treatment on motor symptoms induced by MPTP without affecting depressive-like behaviors and spatial memory (Figures 3J, S3B, and S3C). While the specific reasons behind this phenomenon remain unknown, it is important to note that the morphological and functional heterogeneity of SNc dopaminergic neurons has been documented.<sup>53,54</sup> On one hand, dopaminergic neurons in the lateral SNc, which project to the DS, encode salient signals and play a critical role in regulating motor behaviors.<sup>53,55–57</sup> This aligns with our findings that SNc neurons receiving direct dSC inputs are primarily located in the lateral SNc (Figure S5D), influencing motor symptoms of PD (Figure 6H). On the other hand, dopaminergic neurons in the ventral SNc project to the dorsomedial striatum and encode value signals.<sup>53</sup> Considering this evidence, it is plausible that the observed differential effects of reducing bursting activity in SNc neurons on the effects of bright-light treatment for alleviating various PD symptoms may stem from the functional heterogeneity of SNc dopaminergic neurons.

Although the SC-to-SNc pathway has been proposed across species,<sup>45,58,59</sup> the specific functions of this pathway in the regulation of PD symptoms remain unclear. We demonstrate that activating these SNc-projecting dSC neurons, or SNc dopaminergic neurons receiving direct dSC inputs, can ameliorate motor deficits in MPTP-treated mice (Figures 6D and 6H). Conversely, inhibiting the dSC-to-SNc pathway during bright-light treatment impairs the beneficial effects of this treatment on motor symptoms (Figures 3J and 4H). These findings highlight the pivotal role of the dSC-SNc pathway in mediating the beneficial effects of bright-light

(H) Motor behaviors tested in the OFT, rotarod test, and pole test ( $n = 10–15$  mice/group). All mice received daily i.p. injection of CNO (1 mg/kg) for 2 weeks.  
(I) Pie charts indicating percentage of the three types of SNc dopaminergic neurons receiving direct dSC inputs in different experimental groups ( $n = 28–37$  cells/group).  
Scale bars, 200  $\mu\text{m}$  (B and F). Error bars indicate SEM. One-way ANOVA with Sidak's multiple comparisons test (C, D, G, and H) and chi-squared test (E and I).  
\* $p < 0.05$ , \*\* $p < 0.01$ , \*\*\* $p < 0.001$ ; ns, not significant.

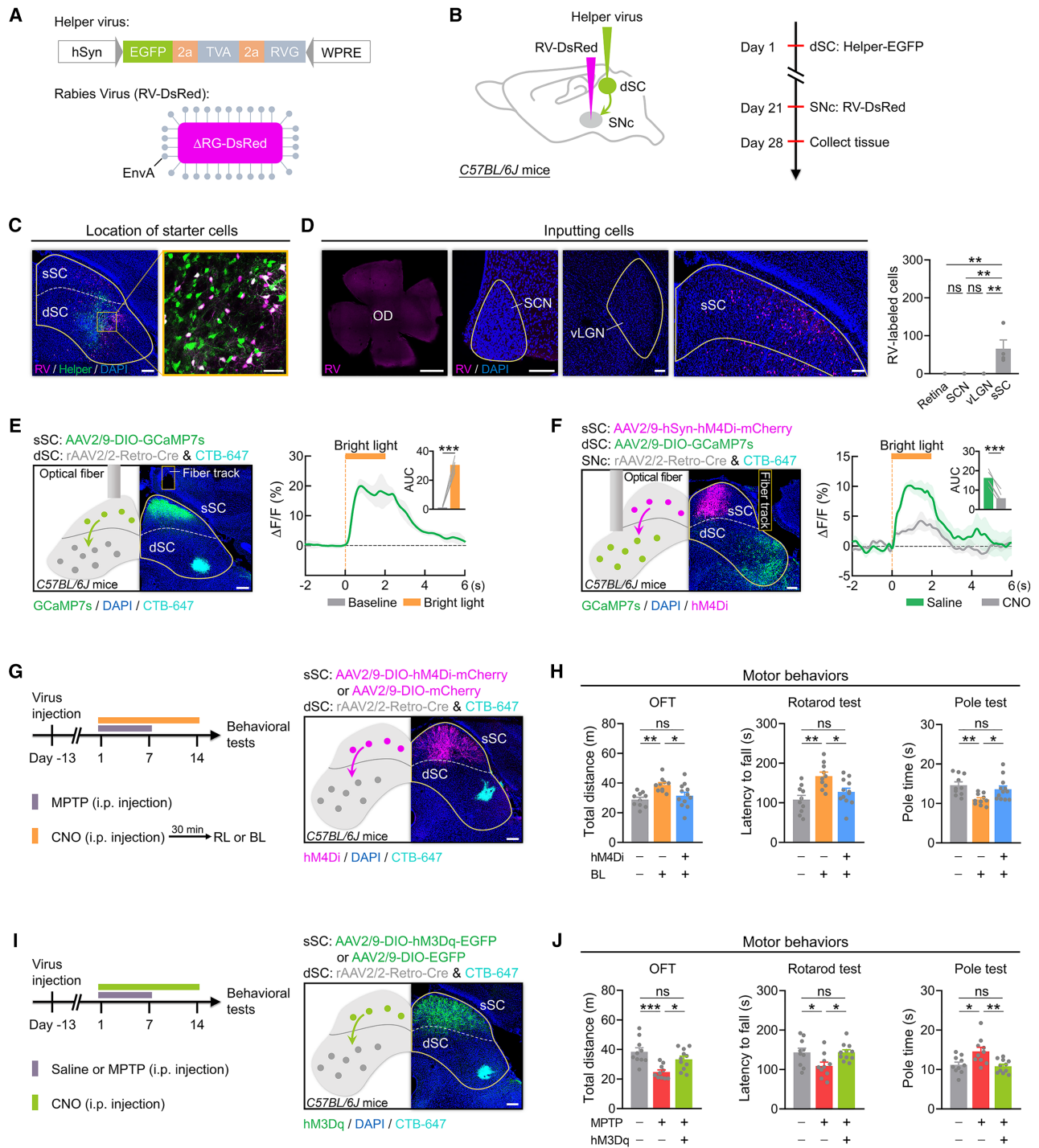


**Figure 7. Activation of dSC-projecting sSC neurons is required for the beneficial effects of bright-light treatment on motor deficits in PD mouse model**

(A) Design of Helper virus and RV-DsRed.

(B) Experimental design of virus tracing in *C57BL/6J* mice.

(C) Injection site of the dSC illustrating the location of starter cells (white).

(D) RV-DsRed-labeled cells in the retina, SCN, vLGN, and sSC.

(E) Left: specific labeling of dSC-projecting sSC neurons with GCaMP7s. Right: average responses and AUC of  $Ca^{2+}$  signals in response to bright-light stimulation ( $n = 5$  mice).

(legend continued on next page)

treatment on motor symptoms. Notably, prior studies have implicated the dSC in regulating sensorimotor transformation and motor functions, such as saccadic eye movements and head movements.<sup>60–62</sup> Interestingly, our results show that specific inhibition of SNc-projecting dSC neurons alone does not significantly affect motor behaviors tested in the OFT, rotarod test, and pole test (Figures S4D and S4E), consistent with previous findings that chemogenetic inhibition of SNc-projecting SC neurons does not affect locomotion in wild-type mice.<sup>58</sup> These results further suggest that the role of SNc-projecting dSC neurons in improving motor symptoms through bright-light treatment is not due to the dSC's inherent ability to regulate motor functions but rather through its modified regulatory effects on the SNc.

In addition to the SNc, research has shown that the dSC can also project to the ventral tegmental area (VTA), which is enriched with dopaminergic neurons and plays a key role in the regulation of diverse brain functions.<sup>63</sup> Notably, recent evidence has identified that distinct subtypes of dSC neurons project to the VTA and SNc, respectively,<sup>58</sup> and that changes in light conditions could also influence neuronal activity in the VTA.<sup>44,64</sup> It is reasonable for one to speculate that the dSC-VTA pathway might also be involved in mediating the effects of bright-light treatment on PD symptoms. However, our data do not support this proposal. We found that chemogenetic inhibition of VTA neurons receiving direct dSC inputs did not significantly alter the effects of bright-light treatment on both non-motor and motor symptoms in MPTP-treated mice (Figures S6E–S6H). These results suggest that even if the dSC-VTA pathway could also transmit bright-light signals, this pathway might mediate the effects of bright light on brain functions other than the depressive-like behaviors, spatial memory, and motor activities tested in this study.

Although SNc-projecting dSC neurons can be activated by bright light (Figure 4D), these neurons receive minimal direct retinal inputs,<sup>65,66</sup> suggesting that light signals are relayed to SNc-projecting dSC neurons via specific visual-related brain regions. It is well documented that the SC, a multilayered midbrain structure essential for sensory information processing, primarily receives visual inputs in the sSC, which then transmits excitation to the dSC neurons.<sup>67–69</sup> Supporting this, we found that a subset of sSC glutamatergic neurons directly innervates the dSC (Figures 7A–7D and S6A) and that bright-light stimulation activates SNc-projecting dSC neurons via the sSC (Figure 7F). We therefore hypothesize that bright-light signals transmitted from the sSC to the dSC could alleviate motor symptoms in a PD mouse model. This hypothesis is supported by our demonstration that activating dSC-projecting sSC neurons improves motor deficits in MPTP-treated mice (Figures 7I and 7J) and that this activation is necessary for the beneficial effects of bright-light treatment on motor symptoms (Figures 7G and 7H). Although it is well established that the sSC

could receive direct inputs from both the retina and the visual cortex,<sup>65,66,70,71</sup> studies have shown that lesions in the visual cortex do not significantly affect the modulation of light on neuronal activity in SNc dopaminergic neurons.<sup>45</sup> Given that retinal ganglion cells predominantly release excitatory glutamate neurotransmitters,<sup>72</sup> it is plausible that bright-light signals activate the sSC-dSC-SNc pathway through direct retinal innervation to improve motor symptoms in the PD mouse model.

Taken together, our study demonstrates that the vLGN- and SNc-related visual pathways are crucial for the beneficial effects of bright-light treatment on the non-motor and motor symptoms of PD, respectively. Activation of the vLGN is both necessary and sufficient for alleviating non-motor symptoms through bright-light treatment, while the sSC-dSC-SNc pathway is essential for improving motor symptoms. Given the conservation of the visual thalamus, the SC, and the SNc across humans and rodents, our findings have the potential to enhance our understanding of the non-image-forming visual functions and provide valuable insights into the neuronal mechanisms by which bright-light therapy ameliorates PD symptoms.

#### Limitations of the study

This study utilized an MPTP-induced PD mouse model to investigate the vLGN- and SC-related neural mechanisms underlying bright-light treatment's efficacy in alleviating PD symptoms. Given the heterogeneity of neuronal types within the vLGN<sup>73</sup> and SC,<sup>74</sup> studies employing precise tools, including refined cell-type-specific Cre lines, are essential to accurately delineate the specific locations of these brain regions and to conduct a more comprehensive and in-depth investigation into the functions of the associated neural pathways. In addition, to facilitate clinical translation, future research should focus on two key directions: (1) validating these findings across diverse PD models, including 6-OHDA and  $\alpha$ -synuclein overexpression models while systematically optimizing bright-light treatment parameters (e.g., wavelength and frequency); and (2) extending the scope of investigation to encompass a broader range of PD-related symptoms, particularly autonomic dysfunction, sleep disorders, and olfactory impairment. Such comprehensive studies incorporating multiple models and symptom domains will provide more robust evidence for establishing light therapy as a viable therapeutic intervention for PD.

#### RESOURCE AVAILABILITY

##### Lead contact

Further information and requests for resources and reagents should be directed to and will be fulfilled by the lead contact, Chaoran Ren ([tchaoran@jnu.edu.cn](mailto:tchaoran@jnu.edu.cn)).

(F) Left: specific labeling of sSC neurons with hM4Di-mCherry and SNc-projecting dSC neurons with GCaMP7s. Right: average responses and AUC of  $\text{Ca}^{2+}$  signals in response to bright-light stimulation ( $n = 5$  mice) in mice that received an i.p. injection of saline or CNO (1 mg/kg).

(G) Left: experimental design. Right: specific infection of dSC-projecting sSC neurons with hM4Di-mCherry or mCherry.

(H) Motor behaviors tested in the OFT, rotarod test, and pole test ( $n = 10$ –12 mice/group). All mice received daily i.p. injection of MPTP (30 mg/kg) for 7 consecutive days and daily i.p. injection of CNO (1 mg/kg) for 2 weeks.

(I) Left: experimental design. Right: specific infection of dSC-projecting sSC neurons with hM3Dq-EGFP or EGFP.

(J) Motor behaviors tested in the OFT, rotarod test, and pole test ( $n = 10$ –11 mice/group). All mice received daily i.p. injection of CNO (1 mg/kg) for 2 weeks.

Scale bars, 50  $\mu\text{m}$  (C [right]), 100  $\mu\text{m}$  (D [middle and right]), 200  $\mu\text{m}$  (C [left], E [left], F [left], G [right], and I [right]), and 1 mm (D [left]). Error bars indicate SEM. One-way ANOVA with Sidak's multiple comparisons test: \* $p < 0.05$ , \*\* $p < 0.01$ , \*\*\* $p < 0.001$ ; ns, not significant. See also Figure S6.

### Materials availability

This study did not generate new unique reagents or new mouse lines.

### Data and code availability

- All data are available in the main text or [supplemental information](#) and will be shared by the [lead contact](#) upon reasonable request.
- This paper does not report original code.
- Any additional information required to reanalyze the data reported in this paper is available from the [lead contact](#) upon request.

### ACKNOWLEDGMENTS

This work was supported by the National Natural Science Foundation of China (32325022, 31922030, 32171010, 31771170, 82172530, 32100820, and 32171009), STI2030-Major Projects (2021ZD0203100), the Guangdong Basic and Applied Basic Research Foundation (2023B1515040010, 2021B1515020035), the Science and Technology Program of Guangdong (2018B030334001), the Science and Technology Program of Guangzhou (202007030012), the Young Elite Scientist Sponsorship Program by CAST (YESS20210181), and the Program of Introducing Talents of Discipline to Universities (B14036). We acknowledge the K.C. Wong Education Foundation.

### AUTHOR CONTRIBUTIONS

C.R., X.H., Q.T., and L.H. designed experiments. C.R., X.H., and Q.T. wrote the manuscript. X.H., S.W., and Z.C. performed behavioral experiments. X.H. and Z.C. performed surgery. X.H. and Z.H. performed physiological recordings. X.H., S.W., Z.C., Y.X., Y.Y., W.Q., L.S., W.-H.H., and S.L. performed histology and microscopy. X.H., S.W., Z.C., S.L., Y.L., and K.-F.S. analyzed the data.

### DECLARATION OF INTERESTS

The authors declare no competing interests.

### STAR★METHODS

Detailed methods are provided in the online version of this paper and include the following:

- [KEY RESOURCES TABLE](#)
- [EXPERIMENTAL MODEL AND SUBJECT DETAILS](#)
  - Mice
- [METHOD DETAILS](#)
  - Surgery and intracranial injection
  - Physiological recording from brain slices
  - Fiber photometry
  - Cannula implantation
  - Western blot
  - Histology and immunocytochemistry
  - Image analysis
  - Behavioral paradigms
  - Quantification of TH immunostaining
  - Quantification of projection density of SNc dopaminergic neurons in the DS
  - Quantification of neurons infected with different viruses
- [QUANTIFICATION AND STATISTICAL ANALYSIS](#)
- [ADDITIONAL RESOURCES](#)

### SUPPLEMENTAL INFORMATION

Supplemental information can be found online at <https://doi.org/10.1016/j.celrep.2025.115865>.

Received: November 12, 2024

Revised: February 24, 2025

Accepted: May 28, 2025

### REFERENCES

1. Foster, R.G., and Hankins, M.W. (2002). Non-rod, non-cone photoreception in the vertebrates. *Prog. Retin. Eye Res.* *21*, 507–527.
2. Fu, Y., Liao, H.W., Do, M.T.H., and Yau, K.W. (2005). Non-image-forming ocular photoreception in vertebrates. *Curr. Opin. Neurobiol.* *15*, 415–422.
3. LeGates, T.A., Fernandez, D.C., and Hattar, S. (2014). Light as a central modulator of circadian rhythms, sleep and affect. *Nat. Rev. Neurosci.* *15*, 443–454.
4. Landgrebe, M., Nyuyki, K., Frank, E., Steffens, T., Hauser, S., Eichhammer, P., Hajak, G., and Langguth, B. (2008). Effects of colour exposure on auditory and somatosensory perception—hints for cross-modal plasticity. *Neuroendocrinol. Lett.* *29*, 518–521.
5. Vandewalle, G., Maquet, P., and Dijk, D.J. (2009). Light as a modulator of cognitive brain function. *Trends Cogn. Sci.* *13*, 429–438.
6. Huang, X., Tao, Q., and Ren, C. (2024). A comprehensive overview of the neural mechanisms of light therapy. *Neurosci. Bull.* *40*, 350–362.
7. Rutten, S., Vriend, C., van den Heuvel, O.A., Smit, J.H., Berendse, H.W., and van der Werf, Y.D. (2012). Bright light therapy in Parkinson's disease: an overview of the background and evidence. *Parkinsons Dis.* *2012*, 767105.
8. Paus, S., Schmitz-Hübsch, T., Wüllner, U., Vogel, A., Klockgether, T., and Abele, M. (2007). Bright light therapy in Parkinson's disease: a pilot study. *Mov. Disord.* *22*, 1495–1498.
9. Willis, G.L., and Turner, E.J.D. (2007). Primary and secondary features of Parkinson's disease improve with strategic exposure to bright light: a case series study. *Chronobiol. Int.* *24*, 521–537.
10. Videnovic, A., Klerman, E.B., Wang, W., Marconi, A., Kuhta, T., and Zee, P. C. (2017). Timed light therapy for sleep and daytime sleepiness associated with Parkinson disease: a randomized clinical trial. *JAMA Neurol.* *74*, 411–418.
11. Lin, F., Su, Y., Weng, Y., Lin, X., Weng, H., Cai, G., and Cai, G. (2021). The effects of bright light therapy on depression and sleep disturbances in patients with Parkinson's disease: a systematic review and meta-analysis of randomized controlled trials. *Sleep Med.* *83*, 280–289.
12. Willis, G.L., Boda, J., and Freelance, C.B. (2018). Polychromatic light exposure as a therapeutic in the treatment and management of Parkinson's disease: a controlled exploratory trial. *Front. Neurol.* *9*, 741.
13. Artemenko, A.R., and Levin, I.I. (1996). The phototherapy of parkinsonism patients. *Zh. Nevrol. Psikhiatr. Im. S S Korsakova* *96*, 63–66.
14. Colwell, C.S. (2011). Linking neural activity and molecular oscillations in the SCN. *Nat. Rev. Neurosci.* *12*, 553–569.
15. Trejo, L.J., and Cicerone, C.M. (1984). Cells in the pretectal olivary nucleus are in the pathway for the direct light reflex of the pupil in the rat. *Brain Res.* *300*, 49–62.
16. Clarke, R.J., and Ikeda, H. (1985). Luminance and darkness detectors in the olivary and posterior pretectal nuclei and their relationship to the pupillary light reflex in the rat. I. Studies with steady luminance levels. *Exp. Brain Res.* *57*, 224–232.
17. Harrington, M.E. (1997). The ventral lateral geniculate nucleus and the intergeniculate leaflet: interrelated structures in the visual and circadian systems. *Neurosci. Biobehav. Rev.* *21*, 705–727.
18. Moore, R.Y. (1989). The geniculohypothalamic tract in monkey and man. *Brain Res.* *486*, 190–194.
19. Niimi, K., Kanaseki, T., and Takimoto, T. (1963). The comparative anatomy of the ventral nucleus of the lateral geniculate body in mammals. *J. Comp. Neurol.* *121*, 313–323.
20. Jones, E.G. (2007). *The Thalamus*, 2nd ed. (Cambridge ; New York: Cambridge University Press).
21. Huang, L., Xi, Y., Peng, Y., Yang, Y., Huang, X., Fu, Y., Tao, Q., Xiao, J., Yuan, T., An, K., et al. (2019). A visual circuit related to habenula underlies

- the antidepressive effects of light therapy. *Neuron (Camb., Mass.)* 102, 128–142.e8.
22. Huang, X., Huang, P., Huang, L., Hu, Z., Liu, X., Shen, J., Xi, Y., Yang, Y., Fu, Y., Tao, Q., et al. (2021). A visual circuit related to the nucleus reuniens for the spatial-memory-promoting effects of light treatment. *Neuron (Camb., Mass.)* 109, 347–362.e7.
  23. Hu, Z., Mu, Y., Huang, L., Hu, Y., Chen, Z., Yang, Y., Huang, X., Fu, Y., Xi, Y., Lin, S., et al. (2022). A visual circuit related to the periaqueductal gray area for the antinociceptive effects of bright light treatment. *Neuron (Camb., Mass.)* 110, 1712–1727.e7.
  24. Fu, Y., Yang, Y., Huang, L., Huang, X., Yang, Q., Tao, Q., Wu, J., So, K.F., Lin, S., Yuan, T.F., and Ren, C. (2023). A visual circuit related to the habenula mediates the prevention of cocaine relapse by bright light treatment. *Sci. Bull. (Beijing)* 68, 2063–2076.
  25. Hu, Z., Huang, X., Liu, J., Wang, Z., Xi, Y., Yang, Y., Lin, S., So, K.F., Huang, L., Tao, Q., and Ren, C. (2024). A visual circuit related to the parabrachial nucleus for the antipruritic effects of bright light treatment. *Cell Rep.* 43, 114356.
  26. Schapira, A.H.V., Chaudhuri, K.R., and Jenner, P. (2017). Non-motor features of Parkinson disease. *Nat. Rev. Neurosci.* 18, 509.
  27. Deumens, R., Blokland, A., and Prickaerts, J. (2002). Modeling Parkinson's disease in rats: an evaluation of 6-OHDA lesions of the nigrostriatal pathway. *Exp. Neurol.* 175, 303–317.
  28. Zhang, Y., Roy, D.S., Zhu, Y., Chen, Y., Aida, T., Hou, Y., Shen, C., Lea, N. E., Schroeder, M.E., Skaggs, K.M., et al. (2022). Targeting thalamic circuits rescues motor and mood deficits in PD mice. *Nature* 607, 321–329.
  29. Diederich, N.J., Uchihara, T., Grillner, S., and Goetz, C.G. (2020). The evolution-driven signature of Parkinson's disease. *Trends Neurosci.* 43, 475–492.
  30. Surmeier, D.J., Obeso, J.A., and Halliday, G.M. (2017). Selective neuronal vulnerability in Parkinson disease. *Nat. Rev. Neurosci.* 18, 101–113.
  31. Grace, A.A., and Bunney, B.S. (1984). The control of firing pattern in nigral dopamine neurons: burst firing. *J. Neurosci.* 4, 2877–2890.
  32. Gonon, F.G. (1988). Nonlinear relationship between impulse flow and dopamine released by rat midbrain dopaminergic neurons as studied by in vivo electrochemistry. *Neuroscience* 24, 19–28.
  33. Panigrahi, B., Martin, K.A., Li, Y., Graves, A.R., Vollmer, A., Olson, L., Mensh, B.D., Karpova, A.Y., and Dudman, J.T. (2015). Dopamine is required for the neural representation and control of movement vigor. *Cell* 162, 1418–1430.
  34. Zhuo, Y., Luo, B., Yi, X., Dong, H., Miao, X., Wan, J., Williams, J.T., Campbell, M.G., Cai, R., Qian, T., et al. (2024). Improved green and red GRAB sensors for monitoring dopaminergic activity in vivo. *Nat. Methods* 21, 680–691.
  35. Overton, P.G., and Clark, D. (1997). Burst firing in midbrain dopaminergic neurons. *Brain Res. Brain Res. Rev.* 25, 312–334.
  36. Holmes, A., Fitzgerald, P.J., MacPherson, K.P., DeBrouse, L., Colacicco, G., Flynn, S.M., Masneuf, S., Pleil, K.E., Li, C., Marcinkiewicz, C.A., et al. (2012). Chronic alcohol remodels prefrontal neurons and disrupts NMDAR-mediated fear extinction encoding. *Nat. Neurosci.* 15, 1359–1361.
  37. Zhang, H., Qian, Y.L., Li, C., Liu, D., Wang, L., Wang, X.Y., Liu, M.J., Liu, H., Zhang, S., Guo, X.Y., et al. (2017). Brain-derived neurotrophic factor in the mesolimbic reward circuitry mediates nociception in chronic neuropathic pain. *Biol. Psychiatry* 82, 608–618.
  38. Pulmanousahakul, R., Li, J., Schnell, M.J., and Dietzschold, B. (2008). The glycoprotein and the matrix protein of rabies virus affect pathogenicity by regulating viral replication and facilitating cell-to-cell spread. *J. Virol.* 82, 2330–2338.
  39. Zingg, B., Chou, X.L., Zhang, Z.G., Mesik, L., Liang, F., Tao, H.W., and Zhang, L.I. (2017). AAV-mediated anterograde transsynaptic tagging: mapping corticocollicular input-defined neural pathways for defense behaviors. *Neuron (Camb., Mass.)* 93, 33–47.
  40. Guo, S.S., Gong, Y., Zhang, T.T., Su, X.Y., Wu, Y.J., Yan, Y.X., Cao, Y., Song, X.L., Xie, J.C., Wu, D., et al. (2024). A thalamic nucleus reuniens-lateral septum-lateral hypothalamus circuit for comorbid anxiety-like behaviors in chronic itch. *Sci. Adv.* 10, eadn6272.
  41. Cruz-Martin, A., El-Danaf, R.N., Osakada, F., Sriram, B., Dhande, O.S., Nguyen, P.L., Callaway, E.M., Ghosh, A., and Huberman, A.D. (2014). A dedicated sleep circuit links direction-selective retinal ganglion cells to the primary visual cortex. *Nature* 507, 358–361.
  42. Tovote, P., Esposito, M.S., Botta, P., Chaudun, F., Fadok, J.P., Markovic, M., Wolff, S.B.E., Ramakrishnan, C., Fenno, L., Deisseroth, K., et al. (2016). Midbrain circuits for defensive behaviour. *Nature* 534, 206–212.
  43. Huang, L., Chen, X., Tao, Q., Wang, X., Huang, X., Fu, Y., Yang, Y., Deng, S., Lin, S., So, K.F., et al. (2023). Bright light treatment counteracts stress-induced sleep alterations in mice, via a visual circuit related to the rostromedial tegmental nucleus. *PLoS Biol.* 21, e3002282.
  44. Dommert, E., Coizet, V., Blaha, C.D., Martindale, J., Lefebvre, V., Walton, N., Mayhew, J.E.W., Overton, P.G., and Redgrave, P. (2005). How visual stimuli activate dopaminergic neurons at short latency. *Sci. Technol. Humanit.* 307, 1476–1479.
  45. Comoli, E., Coizet, V., Boyes, J., Bolam, J.P., Canteras, N.S., Quirk, R.H., Overton, P.G., and Redgrave, P. (2003). A direct projection from superior colliculus to substantia nigra for detecting salient visual events. *Nat. Neurosci.* 6, 974–980.
  46. Qian, D., Li, W., Xue, J., Wu, Y., Wang, Z., Shi, T., Li, S., Yang, J., Qiu, S., Wang, S., et al. (2022). A striatal SOM-driven ChAT-IMSN loop generates beta oscillations and produces motor deficits. *Cell Rep.* 40, 111111.
  47. Howe, M.W., and Dombeck, D.A. (2016). Rapid signalling in distinct dopaminergic axons during locomotion and reward. *Nature* 535, 505–510.
  48. Zhang, Z., Luo, X., Jiang, L., Wu, H., and Tan, Z. (2024). How do HCN channels play a part in Alzheimer's and Parkinson's disease? *Ageing Res. Rev.* 100, 102436.
  49. Guatteo, E., Rizzo, F.R., Federici, M., Cordella, A., Ledonne, A., Latini, L., Nobili, A., Viscomi, M.T., Biamonte, F., Landrock, K.K., et al. (2017). Functional alterations of the dopaminergic and glutamatergic systems in spontaneous alpha-synuclein overexpressing rats. *Exp. Neurol.* 287, 21–33.
  50. Hao, X.M., Xu, R., Chen, A.Q., Sun, F.J., Wang, Y., Liu, H.X., Chen, H., Xue, Y., and Chen, L. (2019). Endogenous HCN channels modulate the firing activity of globus pallidus neurons in parkinsonian animals. *Front. Aging Neurosci.* 11, 190.
  51. Sun, Y., Cao, J., Xu, C., Liu, X., Wang, Z., and Zhao, H. (2020). Rostromedial tegmental nucleus-substantia nigra pars compacta circuit mediates aversive and despair behavior in mice. *Exp. Neurol.* 333, 113433.
  52. Winter, C., von Rumohr, A., Mundt, A., Petrus, D., Klein, J., Lee, T., Morgenstern, R., Kupsch, A., and Juckel, G. (2007). Lesions of dopaminergic neurons in the substantia nigra pars compacta and in the ventral tegmental area enhance depressive-like behavior in rats. *Behav. Brain Res.* 184, 133–141.
  53. Lerner, T.N., Shilyansky, C., Davidson, T.J., Evans, K.E., Beier, K.T., Zolocusky, K.A., Crow, A.K., Malenka, R.C., Luo, L., Tomer, R., and Deisseroth, K. (2015). Intact-brain analyses reveal distinct information carried by SNc dopamine subcircuits. *Cell* 162, 635–647.
  54. Matsumoto, M., and Hikosaka, O. (2009). Two types of dopamine neuron distinctly convey positive and negative motivational signals. *Nature* 459, 837–841.
  55. Le Gratiel, K.L., Anderson, C.K., Puente, N., Grandes, P., Copas, C., Nahirney, P.C., Delaney, K.R., and Nashmi, R. (2022). Differential subcellular distribution and release dynamics of cotransmitted cholinergic and GABAergic synaptic inputs modify dopaminergic neuronal excitability. *J. Neurosci.* 42, 8670–8693.
  56. Markowitz, J.E., Gillis, W.F., Jay, M., Wood, J., Harris, R.W., Cieszkowski, R., Scott, R., Brann, D., Koveal, D., Kula, T., et al. (2023). Spontaneous behaviour is structured by reinforcement without explicit reward. *Nature* 614, 108–117.

57. Young, P.A., Waller, O., Ball, K., Williams, C.C., and Nashmi, R. (2024). Phasic stimulation of dopaminergic neurons of the lateral substantia nigra increases open field exploratory behaviour and reduces habituation over time. *Neuroscience* *551*, 276–289.
58. Huang, M., Li, D., Cheng, X., Pei, Q., Xie, Z., Gu, H., Zhang, X., Chen, Z., Liu, A., Wang, Y., et al. (2021). The tectonigral pathway regulates appetitive locomotion in predatory hunting in mice. *Nat. Commun.* *12*, 4409.
59. Takakuwa, N., Kato, R., Redgrave, P., and Isa, T. (2017). Emergence of visually-evoked reward expectation signals in dopamine neurons via the superior colliculus in V1 lesioned monkeys. *eLife* *6*, e24459.
60. Isa, T., and Sasaki, S. (2002). Brainstem control of head movements during orienting; organization of the premotor circuits. *Prog. Neurobiol.* *66*, 205–241.
61. Wilson, J.J., Alexandre, N., Trentin, C., and Tripodi, M. (2018). Three-dimensional representation of motor space in the mouse superior colliculus. *Curr. Biol.* *28*, 1744–1755.e12.
62. Wang, L., Liu, M., Segraves, M.A., and Cang, J. (2015). Visual experience is required for the development of eye movement maps in the mouse superior colliculus. *J. Neurosci.* *35*, 12281–12286.
63. Morales, M., and Margolis, E.B. (2017). Ventral tegmental area: cellular heterogeneity, connectivity and behaviour. *Nat. Rev. Neurosci.* *18*, 73–85.
64. Zhou, Z., Liu, X., Chen, S., Zhang, Z., Liu, Y., Montardy, Q., Tang, Y., Wei, P., Liu, N., Li, L., et al. (2019). A VTA GABAergic neural circuit mediates visually evoked innate defensive responses. *Neuron (Camb., Mass.)* *103*, 473–488.e6.
65. May, P.J. (2006). The mammalian superior colliculus: laminar structure and connections. *Prog. Brain Res.* *151*, 321–378.
66. Martersteck, E.M., Hirokawa, K.E., Evarts, M., Bernard, A., Duan, X., Li, Y., Ng, L., Oh, S.W., Ouellette, B., Royall, J.J., et al. (2017). Diverse central projection patterns of retinal ganglion cells. *Cell Rep.* *18*, 2058–2072.
67. Isa, T., Endo, T., and Saito, Y. (1998). The visuo-motor pathway in the local circuit of the rat superior colliculus. *J. Neurosci.* *18*, 8496–8504.
68. Helms, M.C., Ozen, G., and Hall, W.C. (2004). Organization of the intermediate gray layer of the superior colliculus. I. Intrinsic vertical connections. *J. Neurophysiol.* *91*, 1706–1715.
69. Kardamakis, A.A., Saitoh, K., and Grillner, S. (2015). Tectal microcircuit generating visual selection commands on gaze-controlling neurons. *Proc. Natl. Acad. Sci. USA* *112*, E1956–E1965.
70. Harvey, A.R., and Worthington, D.R. (1990). The projection from different visual cortical areas to the rat superior colliculus. *J. Comp. Neurol.* *298*, 281–292.
71. Dhande, O.S., and Huberman, A.D. (2014). Retinal ganglion cell maps in the brain: implications for visual processing. *Curr. Opin. Neurobiol.* *24*, 133–142.
72. Finlayson, P.G., and Iezzi, R. (2010). Glutamate stimulation of retinal ganglion cells in normal and s334ter-4 rat retinas: a candidate for a neurotransmitter-based retinal prosthesis. *Investig. Ophthalmol. Vis. Sci.* *51*, 3619–3628.
73. Sabbagh, U., Govindaiah, G., Somaiya, R.D., Ha, R.V., Wei, J.C., Guido, W., and Fox, M.A. (2021). Diverse GABAergic neurons organize into subtype-specific sublaminae in the ventral lateral geniculate nucleus. *J. Neurochem.* *159*, 479–497.
74. Cang, J., Chen, C., Li, C., and Liu, Y. (2024). Genetically defined neuron types underlying visuomotor transformation in the superior colliculus. *Nat. Rev. Neurosci.* *25*, 726–739.

STAR★METHODS

KEY RESOURCES TABLE

REAGENT or RESOURCE	SOURCE	IDENTIFIER
<b>Antibodies</b>		
Rabbit Anti-Tyrosine hydroxylase (TH)	Abcam	Cat# ab6211
Rabbit Anti-Glutamate	Sigma-Aldrich	Cat# G6642
Rabbit Anti-HCN2	Abcam	Cat# ab313873
Rabbit Anti-HCN4	Proteintech	Cat# 55224-1-AP, RRID: AB_11182714
DyLight 488 Donkey Anti-Rabbit	Abcam	Cat# ab150073, RRID: AB_2636877
DyLight 594 Donkey Anti-Rabbit	Jackson ImmunoResearch	Cat# 711-585-152, RRID: AB_2340621
Fluorescent Nissl Stain	Invitrogen	Cat# N21483, RRID: AB_2572212
<b>Bacterial and virus strains</b>		
AAV2/1-hSyn-Cre	Taitool BioScience Co, Shanghai	Cat# S0278-1
rAAV2/2-hSyn-Retro-Cre	Taitool BioScience Co, Shanghai	Cat# S0278-2R
AAV2/1-Flpo	BrainVTA, Wuhan	Cat# PT-0144
AAV2/9-hSyn-hChr2(H134R)-mCherry	Taitool BioScience Co, Shanghai	Cat# S0165-9
AAV2/9-hSyn-jGCaMP7s	Taitool BioScience Co, Shanghai	Cat# S0589-9
AAV2/9-hSyn-DIO-jGCaMP7s	Taitool BioScience Co, Shanghai	Cat# S0590-9
AAV2/9-hSyn-EGFP	BrainVTA, Wuhan	Cat# PT-0241
AAV2/9-hSyn-mCherry	BrainVTA, Wuhan	Cat# PT-0866
AAV2/9-Ef1a-DIO-eYFP	Taitool BioScience Co, Shanghai	Cat# S0196-9
AAV2/9-Ef1a-DIO-mCherry	Taitool BioScience Co, Shanghai	Cat# S0197-9
AAV2/9-hSyn-DIO-hM3D(Gq)-EGFP	Taitool BioScience Co, Shanghai	Cat# S0192-9
AAV2/9-hSyn-hM3D(Gq)-EGFP	Taitool BioScience Co, Shanghai	Cat# S0425-9
AAV2/9-hSyn-DIO-hM4D(Gi)-mCherry	Taitool BioScience Co, Shanghai	Cat# S0193-9
AAV2/9-hSyn-hM4D(Gi)-mCherry	Taitool BioScience Co, Shanghai	Cat# S0279-9
AAV2/9-Ef1a-fDIO-EGFP	BrainVTA, Wuhan	Cat# PT-0435
AAV2/9-Ef1 $\alpha$ -fDIO-hM3D(Gq)-EGFP	BrainVTA, Wuhan	Cat# PT-0160
rAAV-hSyn-EGFP-2A-TVA-2A-RVG-WPREs	BrainVTA, Wuhan	Cat# PT-0022
Rabies virus SAD-DG-DsRed (EnvA)	BrainVTA, Wuhan	Cat# R01002
rAAV-EF1a-DIO-mCherry-TVA	BrainVTA, Wuhan	Cat# PT-0207
rAAV-EF1a-DIO-RVG	BrainVTA, Wuhan	Cat# PT-0023
Rabies virus SAD-DG-EGFP (EnvA)	BrainVTA, Wuhan	Cat# R01001
AAV2/9-hSyn-GRAB <sub>DA</sub>	BrainCase, Shenzhen	Cat# BC-0709
<b>Chemicals, peptides, and recombinant proteins</b>		
1-methyl-4-phenyl-1,2,3,6-tetrahydropyridine (MPTP)	Sigma-Aldrich	Cat# M0896
6-hydroxydopamine (6-OHDA)	Sigma-Aldrich	Cat# H4381
Ascorbic acid 6-palmitate		Cat# A1968
Clozapine N-oxide (CNO)	Abcam	Cat# ab141704
Alexa Fluor 647-conjugated Cholera Toxin Subunit B	ThermoFisher	Cat# C34778
2-amino-5-phosphonovaleric acid (AP5)	Sigma-Aldrich	Cat# 165304
ZD7288	Tocris	Cat# 1000
Mibefradil	Sigma-Aldrich	Cat# M5441
4-aminopyridine (4-AP)	Tocris	Cat# 0940
Tetrodotoxin (TTX)	Tocris	Cat# 1078

(Continued on next page)

**Continued**

REAGENT or RESOURCE	SOURCE	IDENTIFIER
6-cyano-7-nitroquinoxaline-2,3-dione (CNQX)	Tocris	Cat# 0190
Experimental models: Organisms/strains		
Mouse: <i>C57BL/6J</i>	Guangdong Medical Laboratory Animal Center, Guangzhou, China	N/A
Mouse: <i>DAT-Cre</i>	The Jackson Laboratory	Stock No: 006660
Software and algorithms		
Graphpad prism 8	GraphPad Software	<a href="https://www.graphpad.com/">https://www.graphpad.com/</a>
Ethovision XT	Noldus	<a href="https://www.noldus.com/ethovision-xt/">https://www.noldus.com/ethovision-xt/</a>
ImageJ	NIH	<a href="https://imagej.net/ij/">https://imagej.net/ij/</a>
Photoshop CS2023	Adobe	<a href="https://www.adobe.com/products/">https://www.adobe.com/products/</a>
Other		
Light cabinet	Guangzhou Jiuying Bio Technology Co. Ltd	N/A
Fiber photometry system	Inper Ltd., China	N/A
Optical fiber	Thorlabs	FT200UMT
Ceramic ferrule	Fiblaser Technology	N/A

**EXPERIMENTAL MODEL AND SUBJECT DETAILS**

**Mice**

All experiments were approved by the Jinan University Institutional Animal Care and Use Committee. Adult (10–14 weeks old) male *C57BL/6J* and *DAT-Cre* mice were used in this study. The animals were housed in a 12-h light/dark cycle (~200 lux, lights on at 07:00 a.m., corresponding to ZT0) with food and water provided *ad libitum*. The animals were randomly allocated to experimental and control groups. Experimenters were blind to the experimental groups, and the order of testing was counterbalanced during behavioral experiments.

**METHOD DETAILS**

**Surgery and intracranial injection**

Mice were anesthetized (Avertin, 13  $\mu\text{L/g}$ , i.p.) and placed in a stereotaxic instrument (RWD, Shenzhen, China). Erythromycin eye ointment was applied to prevent corneal drying and a heat pad (RWD, Shenzhen, China) was used to hold body temperature at 37°C. Craniotomy holes were drilled with a microdrill (OmniDrill35, WPI, Sarasota, FL) in the skull above the target regions: vLGN (AP: -2.2 mm; ML:  $\pm 2.5$  mm; DV: -3.0 mm), DS (AP: 0.9 mm; ML:  $\pm 2.0$  mm; DV: -2.2 mm), SNc (AP: -2.8 mm; ML:  $\pm 1.25$  mm; DV: -4.5 mm), dSC (AP: -3.9 mm; ML:  $\pm 1.4$  mm; DV: -2.2 mm), sSC (AP: -3.8 mm; ML:  $\pm 0.4$  mm; DV: -1.2 mm), or VTA (AP: -2.8 mm; ML:  $\pm 0.25$  mm; DV: -4.6 mm). Viral vectors were injected through a glass micropipette and controlled by an injector (Microinjection Syringe Pump, WPI) at a speed of 0.1  $\mu\text{L}/\text{min}$ . Following injection, the micropipette was left in place for ~5 min to allow the injectant to diffuse adequately. Mice were allowed to recover from anesthesia under a heat lamp.

For chemogenetic activation or inactivation of all vLGN neurons, AAV2/9-hSyn-hM3Dq-EGFP or AAV2/9-hSyn-hM4Di-mCherry ( $3.5 \times 10^{12}$  GC/mL; 0.1  $\mu\text{L}/\text{injection}$ ) was injected into the vLGN of *C57BL/6J* mice. To selectively activate or inhibit SNc-projecting dSC neurons, rAAV2/2-Retro-Cre ( $3 \times 10^{12}$  GC/mL; 0.1  $\mu\text{L}/\text{injection}$ ) was injected into the SNc, and AAV2/9-DIO-hM3Dq-EGFP or AAV2/9-DIO-hM4Di-mCherry ( $3.5 \times 10^{12}$  GC/mL, 0.1  $\mu\text{L}/\text{injection}$ ) was delivered into the dSC. For selective activation of SNc dopaminergic neurons innervated by dSC, *DAT-Cre* mice received injection of AAV2/1-Flpo ( $1.1 \times 10^{13}$  GC/mL; 0.1  $\mu\text{L}/\text{injection}$ ) into the dSC and AAV2/9-fDIO-hM3Dq-EGFP ( $5.5 \times 10^{12}$  GC/mL; 0.1  $\mu\text{L}/\text{injection}$ ) into the SNc. To chemogenetically modulate dSC-projecting sSC neurons, rAAV2/2-Retro-Cre was injected into the dSC, and AAV2/9-DIO-hM3Dq-EGFP or AAV2/9-DIO-hM4Di-mCherry was injected into the sSC. For all *in vivo* chemogenetic manipulations, mice were intraperitoneally injected with CNO (1 mg/kg). Experimental treatments were conducted 30 min after injection.

To measure neuronal activity in vLGN neurons, AAV2/9-hSyn-GCaMP7s was injected into the vLGN of *C57BL/6J* mice ( $3.5 \times 10^{12}$  GC/mL; 0.1  $\mu\text{L}/\text{injection}$ ). For specific recording of SNc dopaminergic neuron activity, AAV2/9-DIO-GCaMP7s was injected into the SNc of *DAT-Cre* mice ( $3.5 \times 10^{12}$  GC/mL, 0.1  $\mu\text{L}/\text{injection}$ ). To target SNc-projecting dSC neurons with GCaMP7s, rAAV2/2-Retro-Cre was injected into the SNc, AAV2/9-DIO-GCaMP7s was delivered into the dSC (0.1  $\mu\text{L}/\text{injection}$ ). For specific infecting dSC-projecting sSC neurons with GCaMP7s, rAAV2/2-Retro-Cre (0.05  $\mu\text{L}/\text{injection}$ ) was injected into the dSC, AAV2/9-DIO-GCaMP7s was injected into the sSC (0.05  $\mu\text{L}/\text{injection}$ ). To monitor dopamine release in the DS, AAV2/9-hSyn-GRAB<sub>DA</sub> was injected into the DS of

*C57BL/6J* mice ( $2 \times 10^{12}$  GC/mL; 0.2  $\mu$ L/injection). One-week post-injection, an optical fiber (200  $\mu$ m in diameter, numerical aperture = 0.37) was placed 200  $\mu$ m above the injection site and were fixed to the skull with dental cement. Mice were then individually housed and allowed to recover for at least 1 week.

For electrophysiological recording of SNc dopaminergic neurons in response to optogenetic stimulation of the dSC-to-SNc projection, AAV2/9-DIO-eYFP was injected into the SNc of *DAT-Cre* mice, and AAV2/9-hSyn-ChR2-mCherry ( $2.5 \times 10^{12}$  GC/mL, 0.1  $\mu$ L/injection) was injected into the dSC. Two weeks later, the mice were euthanized for patch-clamp recording.

For monosynaptic tracing the inputs to SNc dopaminergic neurons, a total volume of 0.1  $\mu$ L containing an equal volume of AAV2/9-EF1a-DIO-mCherry-TVA ( $2 \times 10^{12}$  GC/mL) and AAV2/9-EF1a-DIO-RVG ( $2 \times 10^{12}$  GC/mL) was injected into the SNc of *DAT-Cre* mice. Twenty-one days later, 0.05  $\mu$ L of SAD-DG-EGFP (EnvA) (RV-EGFP) was injected into the SNc ( $2 \times 10^8$  particles/ml). For disynaptic tracing sSC-dSC-SNc pathway, AAV2/9-hSyn-EGFP-F2A-TVA-T2A-RVG-WPREs (helper) was injected into the dSC ( $3 \times 10^{12}$  GC/mL, 0.05  $\mu$ L/injection). Twenty-one days later, 0.03  $\mu$ L of SAD-DG-DsRed (EnvA) (RV-DsRed) was injected into the SNc ( $3 \times 10^8$  GC/mL).

### Physiological recording from brain slices

For brain slice preparation, the mice were deeply anesthetized with isoflurane, and coronal sections (250  $\mu$ m thick) containing the SNc were cut using a vibratome (VT1200S; Leica Microsystems) in ice-cold artificial cerebrospinal fluid (ACSF, in mM: 119 NaCl; 2.5 KCl, 1  $\text{NaH}_2\text{PO}_4$ , 11 glucose, 26.2  $\text{NaHCO}_3$ , 2.5  $\text{CaCl}_2$ , 1.3  $\text{MgCl}_2$ , 290 mOsm, at pH 7.4). The brain slices were recovered for  $\sim 1$  h at room temperature in N-methyl-D-glucamine-based ACSF (in mM: 93 NMDG, 93 HCl, 2.5 KCl, 1.2  $\text{NaH}_2\text{PO}_4$ , 30  $\text{NaHCO}_3$ , 25 glucose, 20 HEPES, 5 Na-ascorbate, 2 thiourea, 3 Na-pyruvate, 10  $\text{MgSO}_4$ , and 0.5  $\text{CaCl}_2$ , adjusted to 7.35 with HCl). After recovery, the slices were placed in the recording chamber and continuously perfused with ACSF.

Evoked postsynaptic currents were recorded in the eYFP-expressing SNc neurons of *DAT-Cre* mice and were elicited by 5 ms blue-light stimulation of dSC-to-SNc projections infected with ChR2-mCherry. Electrodes were filled with  $\text{Cs}^+$ -based peptide solution (in mM: 130  $\text{CsMeSO}_3$ , 10 NaCl, 10 EGTA, 10  $\text{Na}_2$ -phosphocreatine, 4 MgATP, 0.3  $\text{Na}_3\text{GTP}$ , 10 HEPES, 290 mOsm, adjusted to 7.2 with CsOH). Blue-light-evoked EPSCs and IPSCs were recorded when the membrane potential was held at  $-70$  mV and 0 mV, respectively. To test whether the recorded EPSCs were mediated by the AMPA/kainate receptor, 10  $\mu$ M CNQX was added to ACSF. To test whether the postsynaptic currents recorded in SNc neurons were elicited by direct synaptic connections, 1  $\mu$ M tetrodotoxin (TTX) and 100  $\mu$ M 4-aminopyridine (4-AP) were added to ACSF.

Recordings of spontaneous action potential firing were conducted on SNc neurons expressing eYFP or mCherry in *DAT-Cre* mice. The electrodes were filled with  $\text{K}^+$ -based peptide solution (in mM): 130  $\text{KMeSO}_4$ , 10 KCl, 10 EGTA, 10  $\text{Na}_2$ -phosphocreatine, 4 MgATP, 0.3  $\text{Na}_3\text{GTP}$ , 10 HEPES, 290 mOsm, adjusted to 7.2 with KOH. To evaluate the effects of AP5 (100  $\mu$ M, Sigma), mibefradil (10  $\mu$ M, Sigma), and ZD7288 (50  $\mu$ M, Tocris) on the bursting activity of SNc dopaminergic neurons, these drugs were applied to the ACSF during recordings.

To measure the function of chemogenetic viruses, neurons expressing hM3Dq-EGFP or hM4Di-mCherry in the vLGN, SNc, dSC, sSC or VTA were recorded. For chemogenetic activation, EGFP-labeled neurons were recorded in the current-clamp model. After 80 s of baseline recording, 5  $\mu$ M CNO was washed into ACSF for 50 s, and the neurons were recorded for 4 min in total. For chemogenetic inhibition, mCherry-labeled neurons were injected with a depolarized current, and the number of activated action potentials was calculated as the baseline. Then, 5  $\mu$ M CNO was added to ACSF for 10 min, and the action potentials activated by depolarized current injection were recorded. Finally, the CNO was washed out, and the activated action potentials were recorded.

All recordings were performed using a Multiclamp 700B amplifier (Molecular Devices). Traces were low-pass-filtered at 2 kHz and digitized at 10 kHz. For light stimulation, light pulses were delivered through digital commands from the Digidata 1550A and Digital stimulator (PG4000a, Cygnus Technology). The pipette resistance ranged from 4 to 6  $\text{M}\Omega$ . When stable whole-cell recordings were achieved with an access resistance below 25  $\text{M}\Omega$ , basic electrophysiological properties were recorded. Offline data analysis was performed using Clampfit 10.0 software (Molecular Devices).

### Fiber photometry

For measuring the neuronal activity of vLGN, SNc, dSC and sSC neurons, a fiber photometry system (Inper Ltd., China) was used for recording  $\text{Ca}^{2+}$  signals. Calcium-dependent fluorescence signals were obtained by stimulating neurons expressing GCaMP7s with a 470 nm LED (40  $\mu$ W at fiber tip) while calcium-independent signals were obtained by stimulating these cells with a 410 nm LED (20  $\mu$ W at fiber tip), which was further used to correct for movement artifacts. The 410 nm signal was scaled using least-squares regression to minimize the difference between the 410 nm and 470 nm signal. The fitted 410 nm signal was then subtracted from the 470 nm signal to obtain the movement and bleaching-corrected signal. The fluorescence intensity changes ( $\Delta F/F$ ) were determined by calculating  $(F-F_0)/F_0$ , with  $F_0$  representing the averaged baseline fluorescence signal measured prior to stimulation.

To record the neuronal activity of GCaMP7s-expressed neurons in response to bright-light stimulation, mice were given a 30-min habituation to the testing room with  $\sim 200$  lux white ambient illumination. During recording, bright-light stimulation (3000 lux, 2 s) was delivered with inter-trial intervals of 20 s, and changes in  $\text{Ca}^{2+}$  signals were recorded. For the area under the curve (AUC) calculations, we define the baseline as the 2 s period prior to the onset of bright-light stimulation, AUC was calculated during the 2 s period before or after the onset of bright-light stimulation.

During the recording of  $\text{Ca}^{2+}$  signals in SNc dopaminergic neurons of *DAT-Cre* mice that received dSC injection of AAV2/9-hSyn-hM4Di-mCherry ( $n = 5$  mice), and in SNc-projecting dSC neurons of *C57BL/6J* mice that received sSC injection of AAV2/9-hSyn-hM4Di-mCherry ( $n = 5$  mice), recordings were performed with both CNO and saline on the same animals. Each group of mice received an i.p. injection of either saline or CNO, followed by the alternative treatment 24 h later.

To assess whether bright-light treatment affects dopamine release in the DS of MPTP-treated mice, AAV2/9-hSyn-GRAB<sub>DA</sub> was injected into the DS of *C57BL/6J* mice. Two weeks later, mice were randomly divided into 3 groups: 1) SAL-RL, 5 mice received daily i.p. injection of saline for 7 consecutive days; 2) MPTP-RL, 5 mice received daily i.p. injection of MPTP (30 mg/kg) for 7 consecutive days; 3) MPTP-BL, 5 mice received bright-light treatment, during the first week of which, mice received daily i.p. injection of MPTP (30 mg/kg). Following treatments, mice were placed on a motorized treadmill for a 30-min acclimation period before recordings. Following acclimation, recording started while the mice were still stationary, with running commencing 1 min later. Each mouse ran for 10 s at a speed of 5 m/min. Recordings continued after the treadmill was stopped. All mice underwent 5 trials. We defined the baseline as the 10 s prior to the onset of running, and the traces were z-scored to facilitate comparisons across groups. AUC was calculated during the 10 s period before or after the onset of running.

### Cannula implantation

The surgical procedure was identical to that described for virus injections. Cannulas (RWD Life Science) were bilaterally implanted into the SNc (AP:  $-2.8$  mm, ML:  $\pm 1.3$  mm, DV:  $-4.3$  mm) of the mice. To prevent clogging during the recovery period, a dummy cannula was inserted into the guide cannula. Seven days later, the mice were randomly divided into 4 groups. One group received a daily i.p. injection of MPTP (30 mg/kg) for 7 consecutive days and was designated as the MPTP-RL group. The remaining 3 groups underwent bright-light treatment, with daily MPTP (30 mg/kg) injections administered during the first week and were referred to as the MPTP-BL groups. Pharmacological experiments were conducted following the respective treatments.

For pharmacological experiments, drugs dissolved in ACSF were microinjected using an injector cannula at a rate of  $0.1 \mu\text{L}/\text{min}$ . Following the injection, the cannula was maintained in place for an additional 10 min to minimize drug diffusion along the injection track. Behavioral tests were performed 30 min after the injection of ACSF ( $150 \text{ nL}/\text{site}$ ), AP5 ( $1 \mu\text{g}$ ,  $150 \text{ nL}/\text{site}$ )<sup>36</sup> or ZD7288 ( $0.1 \mu\text{g}$ ,  $150 \text{ nL}/\text{site}$ )<sup>37</sup>. To confirm the drug infusion sites, mice were injected with  $1 \mu\text{L}$  CTB-488 to each side of the SNc after completing all behavioral tests and were euthanized 30 min post-CTB injection. Data analysis included only those mice with correctly localized injections.

### Western blot

SNc tissues were rapidly dissected from  $300 \mu\text{m}$  thick brain slices obtained using a vibratome (VT1200S; Leica Microsystems) and immediately frozen in liquid nitrogen. Total protein from the SNc tissues was then extracted using RIPA lysis buffer (Thermo Fisher Scientific, USA) with phenylmethylsulfonyl fluoride (PMSF; KeyGEN BioTECH, Nanjing). After protein quantification, samples containing  $20 \mu\text{g}$  of protein were separated on an SDS-PAGE gel and subsequently transferred onto a polyvinylidene fluoride (PVDF) membrane. The PVDF membranes were blocked with 5% Bovine Serum Albumin (Biosharp, Beijing) before incubation with primary antibodies overnight at  $4^\circ\text{C}$ . The primary antibodies used were as follows: GAPDH (1:5000, Proteintech, USA), HCN2 (1:500, Abcam, USA), and HCN4 (1:1000, Proteintech, China). Following extensive washing with  $1 \times$  TBST for five cycles, the membranes were incubated with HRP-conjugated secondary antibodies (goat anti-rabbit) for 1 h at room temperature. Band optical intensity was digitized and analyzed using ImageJ software, with the results normalized to GAPDH for accurate quantification.

### Histology and immunocytochemistry

Animals were anesthetized (Avertin,  $13 \mu\text{L}/\text{g}$ , i.p.) and perfused intracardially with 0.9% saline followed by 4% paraformaldehyde in phosphate-buffered saline (PBS). Brains were removed and post-fixed with 4% paraformaldehyde overnight at  $4^\circ\text{C}$ , and then transferred into 30% sucrose until sectioning. A series of  $40 \mu\text{m}$  sections containing target areas were stained with DAPI (ACDbio) or Nissl reagent (NeuroTrace 640/660, Invitrogen) to check the expression of virus, the location of fiber or cannula implantations and viral injections. The Allen brain reference atlas was used to assess anatomical features. To visualize the injection sites of virus did not encode fluorescent protein (i.e., rAAV2/2-Retro-Cre and AAV2/1-Cre), Alexa Fluor 647-conjugated cholera toxin subunit B (CTB-647,  $5 \text{ nL}/\text{injection}$ ) was injected into target regions along with the viruses. Only mice with confirmed expression of virus within the targeted area and verified injection sites were included for data analysis.

For immunostaining, sections were washed in PBS, blocked in blocking buffer, and incubated for 36 h in blocking buffer containing primary antibodies (1:500 dilution) at  $4^\circ\text{C}$ . Sections were then incubated with secondary antibody (1:400 dilution) for 6 h at room temperature, washed again in PBS and cover-slipped in anti-fading aqueous mounting medium with DAPI (EMS, Hatfield, PA).

### Image analysis

Sections were imaged with a Zeiss 700 confocal microscope with  $5\times$  or  $20\times$  objectives. Using ImageJ and Photoshop CS2023 (Adobe Corp., San Jose, California, USA) to adjust contrast and brightness, and the red-green images had been converted to magenta-green.

### Behavioral paradigms

Behavioral tests were performed during the light phase (ZT6 to ZT9) unless otherwise specified. Operators were blinded to the experimental groups during scoring.

#### Bright-light treatment

The animals in both the control and bright-light treatment groups were kept in their home cages which were placed on different layer of a custom-designed light cabinet for different time period (1 week, 2 weeks, or 3 weeks), where all animals were housed at room temperature with *ad libitum* access to food and water. Cool LED lights (UV-free) with adjustable brightness were installed at the top of each floor of the cabinet so that the brightness of each floor of the cabinet could be adjusted manually (the light intensity was determined by averaging the measurements from the top and the four sides of the cage). The animals in the control groups were housed under a 12 h:12 h light/dark cycle (200 lux white ambient illumination). The animals in the experimental groups were also housed under a 12 h:12 h light/dark cycle (200 lux white ambient illumination) except for during bright-light treatment (3000 lux white ambient illumination between ZT1 and ZT3). Following housing in the light cabinet, all animals underwent behavioral tests as detailed below.

#### MPTP-induced PD model

MPTP (M0896, Sigma-Aldrich) was dissolved in sterile saline. Male *C57BL/6J* mice (10–14 weeks old) received i.p. injection of 30 mg/kg MPTP once daily for 7 consecutive days, while mice in the control groups received an equal volume of saline injection on the same schedule. A series of behavioral tests were performed 1 day, 1 week, or 2 weeks after the final MPTP injection. For the bright-light treatment groups, mice were first given daily i.p. injection of MPTP during the initial week, followed by behavioral tests after the bright-light treatment. For mice receiving chemogenetic viral injections in the vLGN, SNc, dSC, sSC, or VTA, daily i.p. injection of MPTP were performed at ZT6, which corresponded to 5.5 h post-CNO injection (1 mg/kg, performed at ZT0.5). After completing the behavioral tests, brain tissue from the mice was collected for further analysis.

#### 6-OHDA-induced PD model

SNc injections of 6-OHDA (H4381, Sigma) were performed using the same methods as those for virus injections. Prior to injecting 6-OHDA, mice were treated with desipramine (25 mg/kg; D3900, Sigma) to increase the selectivity of 6-OHDA-induced lesions. A volume of 300 nL of 6-OHDA (3 mg/mL) dissolved in ice-cold sterile saline containing 0.2% ascorbic acid was injected into the bilateral SNc (AP:  $-2.8$  mm; ML:  $\pm 1.3$  mm; DV:  $-4.5$  mm). Control mice received injections of 300 nL of vehicle (saline with 0.2% ascorbic acid). The 6-OHDA solution was used within 3 h. For the bright-light treatment groups, mice received bright-light treatment following the 6-OHDA injection. Behavioral tests were performed 2 weeks after the surgery.

#### Novel object location recognition (NOL) test

The mice were acclimated to the experimental room for 3 consecutive days prior to the training phase, during which mice were allowed to freely explore the white Plexiglas arena (50 cm length x 50 cm width x 40 cm height) with dim light (15 lux) for 10 min per day. For the training phase, three distinct objects were positioned in 3 corners of the arena 10 cm from the wall. The mice were given 10 min to explore the objects during 6 trials with a 10-min interval between each trial. Memory of the object locations was assessed 24 h after the training phase. During test phase, one of the objects was moved to a diagonal position, and the percentage of time spent by the mice exploring the novel location in 10 min was calculated as the indicator for spatial memory. All objects were pre-screened to ensure no significant preference by the mice. The arena and objects were cleaned with 50% ethanol and dried thoroughly before and between each trial.

#### Morris water maze (MWM) test

Spatial memory was assessed with the hidden platform version of the MWM test. The test apparatus consisted of a large circular pool (diameter 120 cm, depth 70 cm) filled with water (25°C–26°C) to a depth of 40 cm. The water was made opaque with milk to prevent the animals from seeing the circular platform (diameter 12 cm) submerged 1 cm beneath the water surface. The platform was located at a fixed spatial position in one of the quadrants 20 cm from the pool wall. The pool was divided into 4 quadrants with distinct visual cues fixed onto the pool wall.

Twenty-four hours prior to the start of training, all mice were habituated to the pool by allowing them to perform a 60-s swim without the platform. In the following 2 days, the mice were trained to find the hidden platform in a fixed quadrant. Mice received 2 training sessions per day, each of which contained 3 trials. The trials in each session were separated by a 30-min break. For each trial, the mice were gently released into the pool, facing the wall. The mice were given a maximum of 60 s to find the platform. After finding the platform, they were allowed to remain there for 12 s and were then placed in a holding cage until the start of the next trial. The animals that failed to find the platform in 60 s were placed on the platform and allowed to remain there for 12 s. Latency to platform and swimming speed were collected for subsequent analysis. After completion of training, the animals were returned to their home cages until the probe test 24 h later. The probe test consisted of a 60-s free swim period without a platform in which the time spent in the target quadrant was recorded.

#### Sucrose preference test (SPT)

Mice were single housed in the home cage to habituate to two identical bottles containing 2% sucrose solution for 1 day, followed by two identical water bottles for 1 day. Mice were deprived of water for 1 day and then exposed to two bottles, one bottle of water and one bottle of 2% sucrose solution, for 2 h during the dark phase (ZT13 to ZT15), with the locations of bottles reversed at the 1 h time point. Total consumption of water and sucrose solution was measured at the end of the session by weighing the bottles. Sucrose preference was defined as the ratio of the consumption of sucrose solution versus the consumption of both water and sucrose solution.

### Forced swimming test (FST)

Mice were placed in a cylinder of water (23°C–25°C; 20 cm in diameter, 27 cm in height for mice) for 6 min. The depth of water was adjusted to prevent the animals from touching the bottom with their hind limbs. Animal behavior was video-tracked from the side. The time each animal spent immobile during the test was counted online by two independent observers in a blinded manner. Immobility was defined as no active movement except that required to prevent the animal from drowning.

### Open field test (OFT)

Locomotor activity was measured in an open field arena (50 cm length x 50 cm width x 40 cm height). Mice were transferred to the testing room with dim-light condition (15 lux) and acclimatized for 30 min before the test phase. During the testing period, mice were placed in the center of the arena and allowed to explore the arena for 10 min. All animal activity was recorded with an infrared camera placed above the box. Movement of each mouse in the arena was detected using an automated infrared detection system (Ethovision XT software). The apparatus was cleaned with 50% ethanol and dried before and between trials.

### Rotarod test

Mice were transferred to the testing room and acclimatized for 15 min before the test session. They were placed on the rod (Ugo Basile) with the apparatus set to uniform speed of 4 rpm. After a 1-min habituation period, the apparatus was set to uniformly accelerate from 4 rpm to 40 rpm over 5 min. Latency to fall off the rod was recorded for each trial. Each mouse underwent 3 trials with a minimum inter-trial interval of 15 min. The maximum test time for each trial was 300 s, and the fall latency was defined as the average fall latency across the 3 trials. The rod was cleaned with 50% ethanol between trials.

### Pole test

The pole consisted of a wooden cylinder (1 cm in diameter, 50 cm in height) with a wooden ball (2.5 cm in diameter) at the top and a cross-shaped wooden base, all placed in a clean cage. During the test, mice were placed on the wooden ball, and the time taken for each mouse to descend from the ball to the base of the pole was recorded. Each mouse underwent 3 trials with a minimum inter-trial interval of 15 min. The average time across the three trials was used as the statistical indicator. Trials were excluded if the mouse jumped or slid down the pole rather than descended in a climbing manner. The pole was cleaned with 50% ethanol between trials.

### Quantification of TH immunostaining

To quantify the influence of bright-light treatment on MPTP-induced death of SNc dopaminergic neurons. 21 *C57BL/6J* mice were divided into 3 groups: 1) SAL-RL, 7 mice received daily i.p. injection of saline for 7 consecutive days; 2) MPTP-RL, 7 mice received daily i.p. injection of MPTP (30 mg/kg) for 7 consecutive days; 3) MPTP-BL, 7 mice received bright-light treatment, during the first week of which, mice received daily i.p. injection of MPTP (30 mg/kg). All animals were anesthetized and perfused 1 week after the last injection. Brain tissues were subjected to immunostaining of TH. In each mouse, the total number of TH labeled SNc neurons were counted in three serial brain sections (40  $\mu\text{m}$ /section) across the SNc.

### Quantification of projection density of SNc dopaminergic neurons in the DS

To quantify the influence of bright-light treatment on MPTP-induced decreased projection density of SNc dopaminergic neurons in the DS, AAV2/9-DIO-eYFP was injected into the SNc of 18 *DAT-Cre* mice. Two weeks later, the mice were divided into 3 groups: 1) SAL-RL, 6 mice received daily i.p. injection of saline for 7 consecutive days; 2) MPTP-RL, 6 mice received daily i.p. injection of MPTP (30 mg/kg) for 7 consecutive days; 3) MPTP-BL, 6 mice received bright-light treatment, during the first week of which, mice received daily i.p. injection of MPTP (30 mg/kg). All animals were anesthetized and perfused 1 week after the last injection. Brain tissues were collected and the projection density of the SNc dopaminergic neurons in the DS was quantified using ImageJ software. The optical density from the overlying corpus callosum was used as a background and subtracted from every measurement in the DS. In each mouse, the optical density was averaged across three serial brain sections (40  $\mu\text{m}$ /section) within the DS and then normalized to the mean value from the SAL-RL group.

### Quantification of neurons infected with different viruses

To quantify percentage of SNc-projecting dSC neurons co-labeled with eYFP and glutamate (Figure S5C), 4 *C57BL/6J* mice received SNc injection of rAAV2/2-Retro-Cre and dSC injection of AAV2/9-DIO-eYFP were used. In each mouse, the number of eYFP and glutamate double labeled dSC neurons were counted in three serial brain sections (40  $\mu\text{m}$ /section) across the dSC. The percentage of eYFP and glutamate double labeled neurons was calculated as a percentage of the total number of eYFP and glutamate double labeled neurons counted in 4 mice from the total number of eYFP-labeled neurons counted in 4 mice.

To quantify percentage of postsynaptic SNc neurons co-labeled with eYFP and TH (Figure S5F), 4 *C57BL/6J* mice received dSC injection of AAV2/1-Cre and SNc injection of AAV2/9-DIO-eYFP were used. In each mouse, the number of eYFP and TH double labeled neurons were counted in three serial brain sections (40  $\mu\text{m}$ /section) across the SNc. The percentage of eYFP/TH double labeled neurons was calculated as a percentage of the total number of eYFP/TH double labeled neurons counted in 4 mice from the total number of eYFP-labeled neurons counted in 4 mice.

To quantify percentage of RV-DsRed labeled sSC neurons co-labeled with dsRed and glutamate (Figure S6A), 4 *C57BL/6J* mice received dSC injection of helper virus and SNc injection of RV-DsRed were used. In each mouse, the number of RV-DsRed-labeled sSC neurons and RV-DsRed/glutamate double labeled sSC neurons were counted in three serial brain sections (40  $\mu\text{m}$ /section) across the sSC. The percentage of RV-DsRed/glutamate double labeled sSC neurons was calculated as a percentage of the total

number of RV-DsRed/glutamate double labeled sSC neurons counted in 4 mice from the total number of RV-DsRed-labeled sSC neurons counted in 4 mice.

### QUANTIFICATION AND STATISTICAL ANALYSIS

All statistics were calculated using GraphPad Prism 8 software (San Diego, CA, USA). Data analysis was done by experimenters who were blind to experimental conditions. One-way ANOVA followed by *Sidak's* multiple comparisons test was used to quantify the performance of the SPT, FST, NOL, MWM, OFT, rotarod and pole tests. Chi-square test was used to quantify the percentage of burst-firing cells. For all figures, dot plots include horizontal line representing mean. Statistical significance was set at  $p < 0.05$ .

### ADDITIONAL RESOURCES

No new resources or clinical trials were generated in this study.

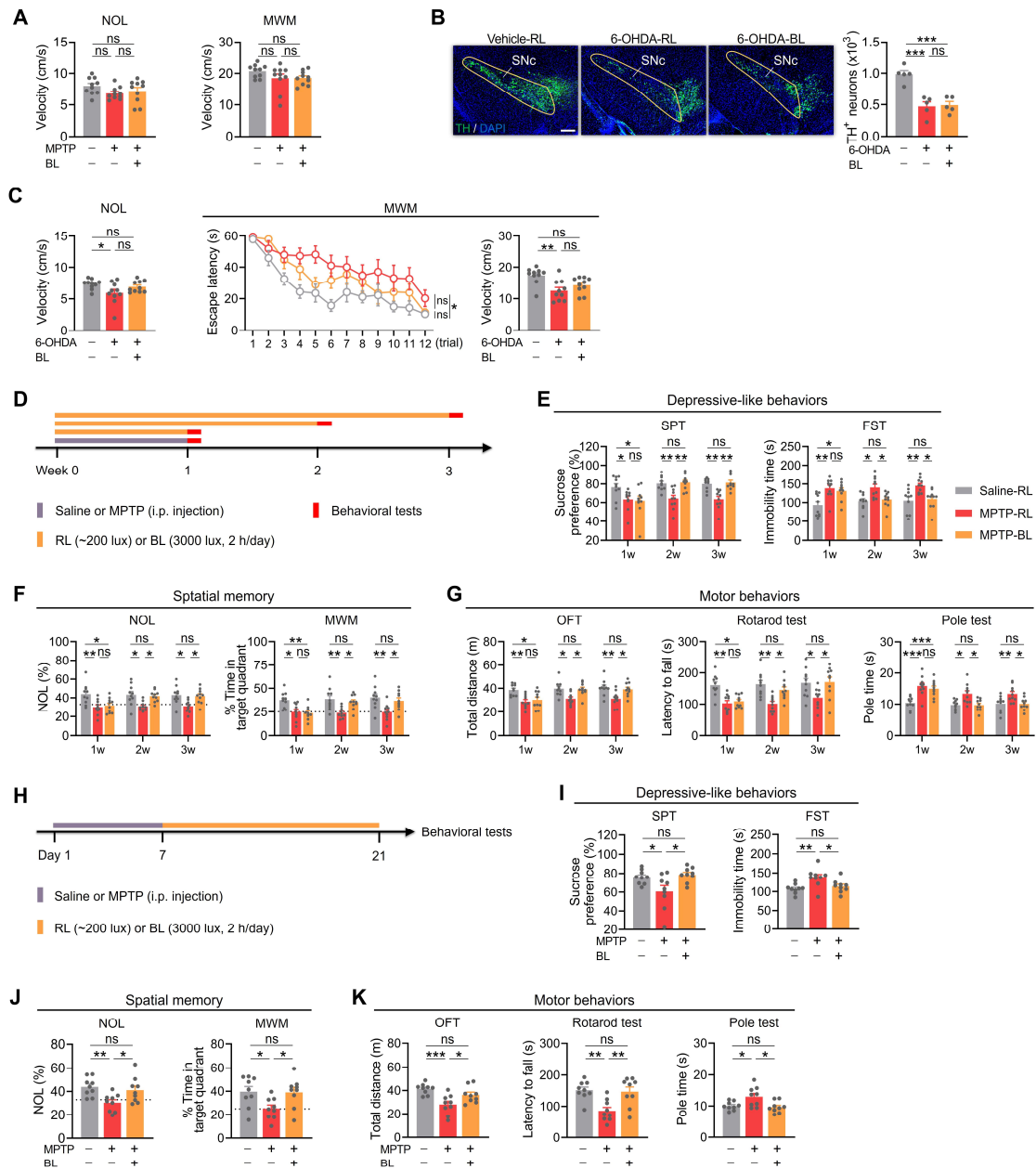
**Cell Reports, Volume 44**

**Supplemental information**

**Bright-light treatment ameliorates motor and  
non-motor deficits through distinct visual  
circuits in a mouse model of Parkinson's disease**

**Xiaodan Huang, Shengnan Wang, Zhiqing Chen, Wenna Qu, Li Song, Zhengfang Hu, Yue Xi, Yan Yang, Weng-Hei Hong, Song Lin, Kwok-Fai So, Yulong Li, Lu Huang, Qian Tao, and Chaoran Ren**

# 1 Supplementary Figures



2

3 **Figure S1. Bright light treatment alleviates depressive-like behaviors, enhances spatial**

4 **memory, and improves motor deficits in PD mouse models, Related to Figure 1. (A) Average**

5 **velocity during the NOL and the probe test of the MWM ( $n = 10$  mice/group). (B) Representative**

6 **images and the number of SNc TH<sup>+</sup> neurons in different experimental groups ( $n = 5$  mice/group).**

7 **(C) Average velocity during the NOL, escape latency and average velocity in the MWM ( $n = 10$**

8 **mice/group). (D) Experimental design. (E-G) Depressive-like behaviors tested in the SPT and FST**

9 (E), spatial memory tested in the NOL and MWM (F), and motor behaviors tested in the OFT,  
10 rotarod test and pole test (G) ( $n = 10$  mice/group). (H) Experimental design. (I-K) Depressive-like  
11 behaviors tested in the SPT and FST (I), spatial memory tested in the NOL and MWM (J), and motor  
12 behaviors tested in the OFT, rotarod test and pole test (K) ( $n = 9$  mice/group). Scale bar: 100  $\mu\text{m}$   
13 (B). For all figures: one-way ANOVA with *Sidak's* multiple-comparisons test,  $*p < 0.05$ ,  $**p < 0.01$ ,  
14  $***p < 0.001$ , ns = not significant. Error bars indicate the SEM.

15

16

17

18

19

20

21

22

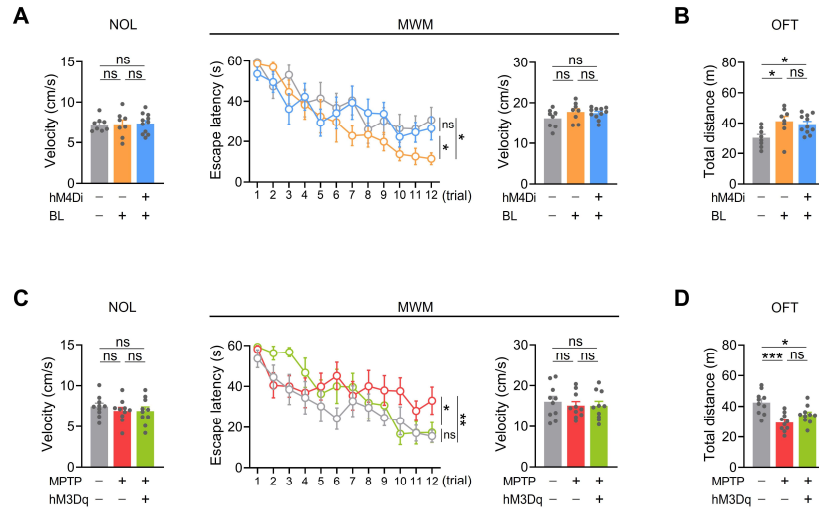
23

24

25

26

27



28

29 **Figure S2. Effects of chemogenetic inhibition/activation of vLGN neurons on locomotor**

30 **activities during the NOL and MWM tests, Related to Figure 2. (A) Average velocity during the**

31 **NOL, escape latency and average velocity in the MWM ( $n = 8-10$  mice/group). All mice received**

32 **daily i.p. injection of MPTP (30 mg/kg) for 7 consecutive days and daily i.p. injection of CNO (1**

33 **mg/kg) for 2 weeks. (B) Total distance traveled during the OFT ( $n = 8-10$  mice/group). (C) Average**

34 **velocity during the NOL, escape latency and average velocity in the MWM ( $n = 10$  mice/group).**

35 **All mice received daily i.p. injection of CNO (1 mg/kg) for 2 weeks and exposure to room light (RL,**

36 **200 lux) during the daytime. (D) Total distance traveled during the OFT ( $n = 10$  mice/group). For**

37 **all figures: one-way ANOVA with *Sidak's* multiple-comparisons test,  $*p < 0.05$ ,  $**p < 0.01$ ,  $***p <$**

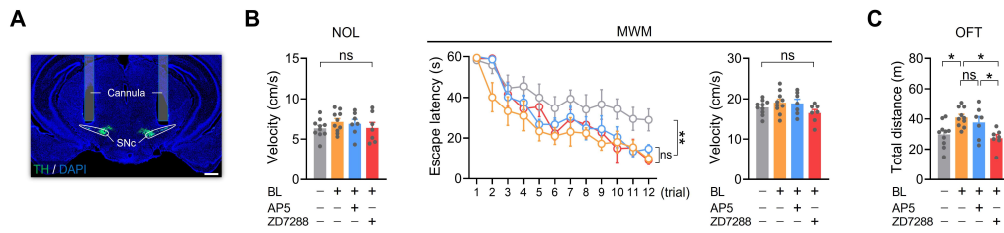
38 **0.001, ns = not significant. Error bars indicate the SEM.**

39

40

41

42



43

44 **Figure S3. Effects of inhibiting bursting activity in SNc neurons on locomotor activities during**

45 **the NOL and MWM tests, Related to Figure 3. (A) A representative image showing the bilateral**

46 **cannula implantation in the SNc of *C57BL/6J* mice. (B) Average velocity during the NOL, escape**

47 **latency and average velocity in the MWM ( $n = 7-10$  mice/group). All mice received daily i.p.**

48 **injection of MPTP (30 mg/kg) for 7 consecutive days and received an infusion of drug into the SNc**

49 **30 min prior to behavioral tests. (C) Total distance traveled during the OFT ( $n = 7-10$  mice/group).**

50 **Scale bar: 500  $\mu$ m (A). For all figures: one-way ANOVA with *Sidak's* multiple-comparisons test,  $*p$**

51  **$< 0.05$ ,  $**p < 0.01$ , ns = not significant. Error bars indicate the SEM.**

52

53

54

55

56

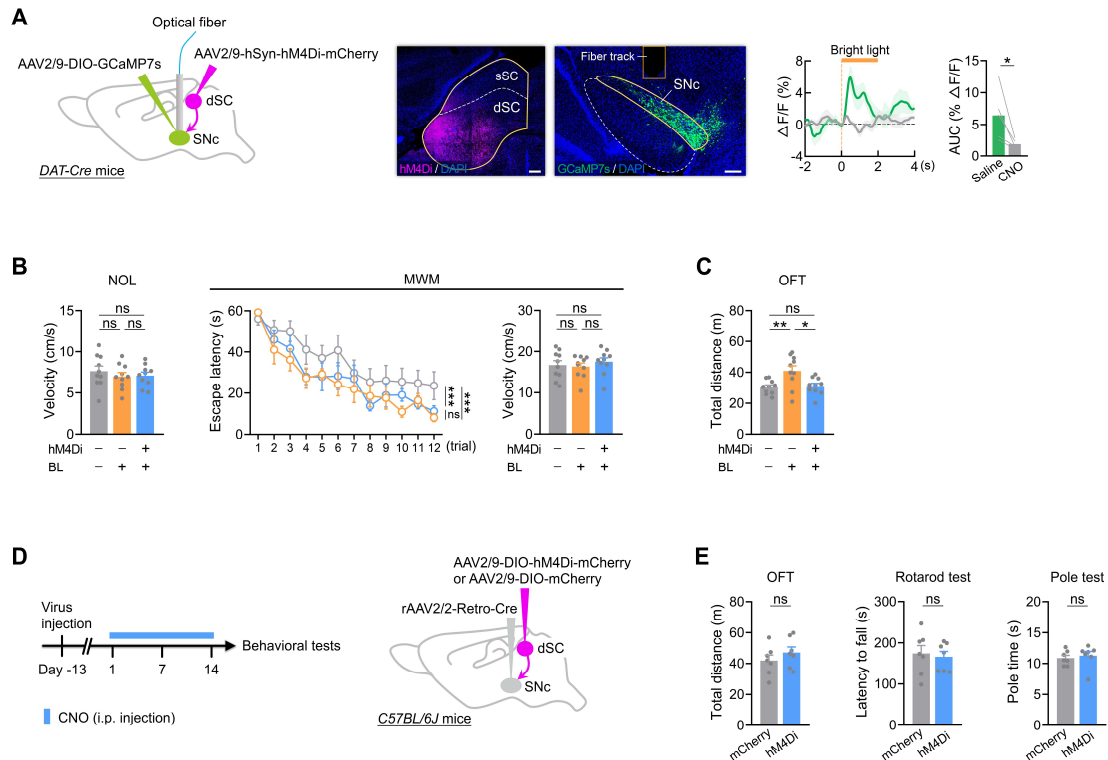
57

58

59

60

61



62

63 **Figure S4. Effects of inhibition of SNc-projecting dSC neurons on motor behaviors tested in**

64 **the OFT, rotarod and pole test, Related to Figure 4. (A) Left: scheme for specific labeling of dSC**

65 **neurons with hM4Di-mCherry and SNc dopaminergic neurons with GCaMP7s in *DAT-Cre* mice.**

66 **Middle: representative images of the dSC and SNc 2 weeks after virus injections. Right: average**

67 **responses and area under the curve (AUC) of  $Ca^{2+}$  signals in response to bright light stimulation**

68 **(3000 lux, 2 s/trial;  $n = 5$  mice) in mice received an i.p. injection of saline or CNO (1 mg/kg). (B)**

69 **Average velocity during the NOL, escape latency and average velocity in the MWM ( $n = 10$**

70 **mice/group). All mice received daily i.p. injection of MPTP (30 mg/kg) for 7 consecutive days and**

71 **daily i.p. injection of CNO (1 mg/kg) for 2 weeks. (C) Total distance traveled during the OFT ( $n =$**

72 **10 mice/group). (D) Left: experimental design. Right: scheme for specific labeling SNc-projecting**

73 **dSC neurons with hM4Di-mCherry or mCherry. (E) Motor behaviors tested in the OFT, rotarod test**

74 **and pole test ( $n = 7$  mice/group). All mice received daily i.p. injection of CNO (1 mg/kg) for 2 weeks.**

75 **Scale bars: 100  $\mu$ m (A-right); 200  $\mu$ m (A-left). For all figures: one-way ANOVA with *Sidak's***

76 multiple-comparisons test,  $*p < 0.05$ ,  $**p < 0.01$ ,  $***p < 0.001$ , ns = not significant. Error bars

77 indicate the SEM.

78

79

80

81

82

83

84

85

86

87

88

89

90

91

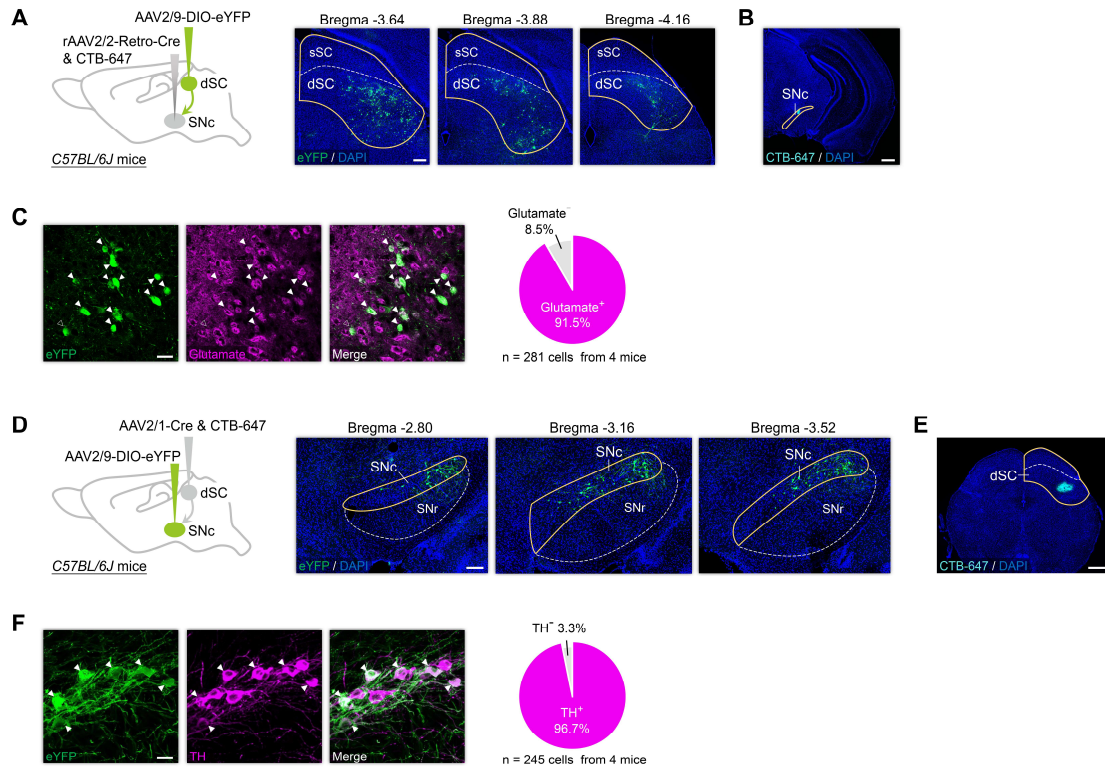
92

93

94

95

96



97

98 **Figure S5. dSC glutamate<sup>+</sup> neurons synapse onto SNc TH<sup>+</sup> neurons, Related to Figure 5. (A)**

99 A schematic diagram (left) and representative images (right) illustrate SNc-projecting dSC neurons

100 labeled with eYFP, with numbers indicating the distance from bregma. (B) The location of the

101 injection site of rAAV2/2-Retro-Cre was visualized with CTB-647. (C) Left: representative images

102 of the dSC illustrating eYFP-expressing dSC neurons co-labeled with glutamate. Right: pie chart

103 indicating percentage of eYFP-expressing dSC neurons co-labeled with glutamate. (D) A schematic

104 diagram (left) and representative images (right) illustrate SNc postsynaptic neurons labeled with

105 eYFP, with numbers indicating the distance from bregma. (E) The location of the injection site of

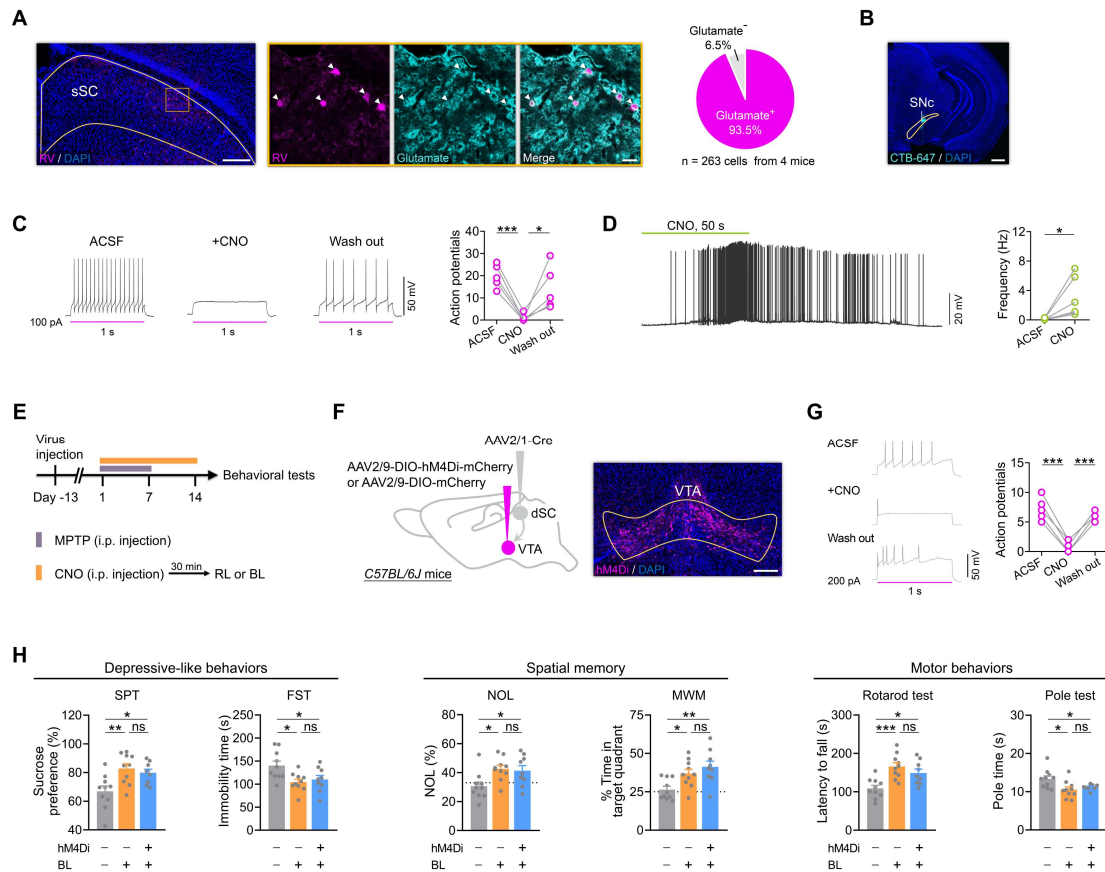
106 AAV2/1-Cre was visualized with CTB-647. (F) Left: representative images of the SNc illustrating

107 eYFP-expressing SNc postsynaptic neurons co-labeled with TH. Right: pie chart indicating

108 percentage of eYFP-expressing SNc neurons co-labeled with TH. Scale bars: 20  $\mu$ m (C, F); 100  $\mu$ m

109 (D); 200  $\mu$ m (A); 500  $\mu$ m (B, E).

110



111

112 **Figure S6. Activation of VTA neurons receiving direct dSC inputs are not required for the**

113 **beneficial effects of bright light treatment on PD symptoms, Related to Figure 7. (A) Left: a**

114 **representative image of the sSC showing RV-DsRed-labeled neurons. Middle: representative images**

115 **of the sSC showing RV-DsRed-labeled neurons that were co-labeled with glutamate. Right: pie chart**

116 **indicating percentage of RV-DsRed-labeled sSC neurons co-labeled with glutamate. (B) The**

117 **location of the injection site of rAAV2/2-Retro-Cre was visualized with CTB-647. (C) Functional**

118 **validation of chemogenetic inhibition in dSC-projecting sSC neurons expressing hM4Di (CNO, 5**

119 **μM). ACSF, artificial cerebrospinal fluid. (D) Functional validation of chemogenetic activation in**

120 **dSC-projecting sSC neurons expressing hM3Dq (CNO, 5 μM). (E) Experimental design. (F)**

121 **Specific labeling of VTA neurons receiving direct dSC inputs with hM4Di-mCherry or mCherry.**

122 **(G) Functional validation of chemogenetic inhibition in hM4Di-expressing VTA neurons receiving**

123 **direct dSC inputs (CNO, 5 μM). (H) Depressive-like behaviors tested in the SPT and FST, spatial**

124 memory tested in the NOL and MWM, and motor behaviors tested in the rotarod test and pole test  
125 ( $n = 9-10$  mice/group). All mice received daily i.p. injection of MPTP (30 mg/kg) for 7 consecutive  
126 days and daily i.p. injection of CNO (1 mg/kg) for 2 weeks. Scale bars: 20  $\mu\text{m}$  (A-middle); 200  $\mu\text{m}$   
127 (A-left, F); 500  $\mu\text{m}$  (B). For all figures: one-way ANOVA with *Sidak's* multiple-comparisons test,  
128  $*p < 0.05$ ,  $**p < 0.01$ ,  $***p < 0.001$ , ns = not significant. Error bars indicate the SEM.

129

130

131

132

133

134

135

136

137

138

139

140

141

142

143

144

145

Brain areas	
DS	Dorsal striatum
dSC	Deep layers of the superior colliculus
LHb	Lateral habenula
OPN	Olivary pretectal nucleus
Re	Nucleus reuniens
RGCs	Retinal ganglion cells
SC	Superior colliculus
SCN	Suprachiasmatic nucleus
SNC	Substantia nigra pars compacta
sSC	Superficial layers of the superior colliculus
vLGN	Ventral lateral geniculate nucleus
VTA	Ventral tegmental area
Behavioral tests	
FST	Forced swimming test
MWM	Morris water maze
NOL	Novel location recognition test
OFT	Open field test
SPT	Sucrose preference test
Chemicals	
AP5	2-amino-5-phosphonovaleric acid
CNO	Clozapine N-oxide
CNQX	6-cyano-7-nitroquinoxaline-2,3-dione
MPTP	1-methyl-4-phenyl-1,2,3,6-tetrahydropyridine
NMDG	N-methyl-D-glucamine
TTX	Tetrodotoxin
4-AP	4-aminopyridine
6-OHDA	6-hydroxydopamine
Other	
AAVs	Adeno-associated virus
ACSF	Artificial cerebrospinal fluid
AUC	Area under the curve
BL	Bright light
ChR2	Channelrhodopsin-2
CTB-488/647	Alexa Fluor 488/647-conjugated cholera toxin subunit B
DREADDs	Designer receptors exclusively activated by designer drugs
EGFP	Enhanced green fluorescent protein
EPSCs	Excitatory postsynaptic currents
eYFP	Enhanced yellow fluorescent protein
Flpo	Flippase

GCaMP7s	Genetically encoded green fluorescent protein calcium indicators
GRAB-DA sensor	GPCR-activation-based dopamine sensor
HCN channels	Hyperpolarization-activated cyclic nucleotide-gated channels
hSyn	human Synapsin
i.p. injection	intraperitoneal injection
IPSCs	Inhibitory postsynaptic currents
NMDARs	N-methyl-d-aspartate receptors
PBS	Phosphate-buffered saline
PD	Parkinson's disease
PMSF	Phenylmethylsulfonyl fluoride
PVDF	Polyvinylidene fluoride
RL	Room light
TBST	Tris buffered saline with Tween 20
TH	Tyrosine hydroxylase
T-VSCCs	Voltage-sensitive T-type calcium channels
ZT	Zeitgeber time